UNIVERSITÀ DEGLI STUDI DI PADOVA

DIPARTIMENTO DI BIOLOGIA

Corso di Laurea in Biologia Molecolare

ELABORATO DI LAUREA

ALTERAZIONI DELLA RISPOSTA AL DANNO DEL DNA ASSOCIATE ALLE INCLUSIONI CITOPLASMATICHE DI TDP-43 E FUS MUTANTE: MECCANISMI MOLECOLARI E STRATEGIE DI RECUPERO FARMACOLOGICO

Tutor Prof. Marco Bisaglia
Dipartimento di Biologia

Laureanda: Arianna Sissa

ANNO ACCADEMICO 2025/2026

INDICE

GLOSSARIO

CIs: Inclusioni citoplasmatiche
DBS: Rottura a doppio filamento del DNA
DDR: Risposta al danno del DNA
fALS: SLA famigliare
FUS: *Fused in sarcoma*
iPSC: Cellule staminali pluripotenti indotte
NCS: Neocarzinostatina
SGs: Granuli da stress
SLA: Sclerosi laterale amiotrofica
sALS: SLA sporadica
SSB: Rottura a singolo filamento del DNA
TDP-43: *TAR DNA-binding protein 43*

ABSTRACT

La sclerosi laterale amiotrofica è una malattia neurodegenerativa progressiva che causa debolezza muscolare e difficoltà motorie fino alla paralisi completa dei muscoli volontari. È caratterizzata dalla formazione di inclusioni citoplasmatiche di TDP-43 e FUS e dall'accumulo di danni al DNA nei motoneuroni.

Nello studio è stato analizzato come gli aggregati intracellulari, colocalizzati con i granuli da stress, portino a un'attivazione disfunzionale della risposta al danno del DNA, causando rotture a doppio filamento del DNA accompagnate da una ridotta sintesi di RNA.

Usando *Drosophila melanogaster* come modello sperimentale, è stato visto che l'inibizione dell'attività della chinasi DDR ATM, ma non di ATR, abolisce la segnalazione di risposta al danno del DNA, indicando che le rotture a doppio filamento del DNA sono la fonte primaria di attivazione della risposta al danno del DNA.

Inoltre, è stato dimostrato che le endoribonucleasi DROSHA e DICER, in grado di interagire con TDP-43 e FUS durante il processamento dei piccoli RNA, contribuiscono alla segnalazione sulla DDR nelle rotture a doppio filamento del DNA.

Nelle cellule coltivate con inclusioni citoplasmatiche e in un modello murino è stato scoperto che l'enoxacina stimola la DDR e la riparazione potenziando l'attività enzimatica di DICER, ripristina una DDR efficiente e riduce l'accumulo di danni al DNA.

INTRODUZIONE

Ruolo di TDP-43 e FUS nella patogenesi della sclerosi laterale amiotrofica

La sclerosi laterale amiotrofica (SLA) è definita una proteinopatia poiché i motoneuroni dei pazienti affetti da questa patologia presentano aggregati proteici nel loro citoplasma. [1] Il 90% dei casi di SLA è sporadico (sALS), mentre il restante 10% presenta un'eredità familiare (fALS) dovuta a mutazioni autosomiche dominanti, autosomiche recessive o legate all'X a carico di geni specifici. Il 4-5% dei casi di fALS e il 2% dei casi di sALS possiedono una mutazione nel gene *TARDBP* che codifica per la proteina TDP-43 (TAR DNA-binding protein 43), mentre il 4% dei casi di fALS e l'1% dei casi di sALS nel gene *FUS* (fused in sarcoma). Entrambe queste mutazioni spesso seguono un modello di ereditarietà autosomica dominante. [1,2]

Sia TDP-43 che FUS sono coinvolte nella biogenesi dei microRNA attraverso la loro interazione con l'endoribonucleasi DROSHA. Entrambe sono inoltre strutturalmente caratterizzate dalla presenza di domini che permettono alle due proteine di subire separazione di fase liquido-liquido, essenziale per la formazione di organelli insolubili privi di membrana, quali i granuli da stress (SGs). La proteina FUS mostra anche un ruolo regolatorio trascrizionale e può legarsi direttamente al dominio C-terminale della RNA polimerasi II. [1]

I SGs vengono generati in risposta a diverse fonti di stress, con la funzione proposta di sospendere la sintesi proteica fino alla fine dello stress. Insieme ai loro componenti classici, TIA-1 e G3BP1, i SGs possono includere TDP-43 e FUS. I motoneuroni derivati da cellule staminali pluripotenti indotte portatrici della mutazione FUS^{P525L} mostrano un numero aumentato e una cinetica alterata nell'assemblaggio dei SG. [1] (Fig. 1J) Si ritiene quindi che le mutazioni, in particolare quella di FUS^{P525L}, aumentino la predisposizione delle cellule a formare aggregati citosolici. Tuttavia, nella maggioranza dei casi, sia di fALS che di sALS TDP-43 si accumula in inclusioni citoplasmatiche (CIs) sia nella forma wild-type che nella forma mutata.

La SLA è stata anche associata a un elevato accumulo di lesioni del DNA nel nucleo dei motoneuroni, compromettendo la loro vitalità: ciò è dovuto a un errore nella risposta al danno del DNA (DDR) che di norma rileva immediatamente la lesione del DNA, ne segnala la formazione e assicura una corretta riparazione dello stesso. In particolare, in presenza di una rottura a doppio filamento (DSB), il complesso multiproteico MRN si lega alle estremità del DNA, reclutando e attivando ATM, un membro della famiglia delle chinasi correlate alla fosfatidilinositolo 3-chinasi (PIKK). ATM, a sua volta, avvia il segnale DDR fosforilando la variante istonica H2AX, che nella sua versione fosforilata è chiamata γH2AX. In caso di accumulo di rotture a singolo filamento (SSBs), generalmente durante lo stress replicativo,

H2AX viene fosforilata da ATR, un'altra PIKK. La marcatura iniziale della cromatina con γH2AX crea un circuito di feedback positivo che alimenta l'ulteriore diffusione di γH2AX e l'accumulo sequenziale di proteine DDR, tra cui 53BP1, che svolge un ruolo fondamentale nell'orchestrare la scelta delle vie di riparazione dei DSB. [1] (Fig. 1H)

Aspetti patologici delle mutazioni in FUS

Il locus associato ad ALS6 è stato mappato sul cromosoma 16p11.2, che codifica il gene FUS. I pazienti affetti da SLA con mutazioni ALS6 sono caratterizzati da un'ampia variabilità nell'età di insorgenza della malattia, compresa tra 26 e 80 anni, con una durata media di circa 33 mesi. Nella maggior parte dei casi si osserva una predominanza del coinvolgimento dei motoneuroni inferiori (LMN), senza interessamento della regione bulbare né compromissione cognitiva. [2].

In vari organismi modello, le mutazioni di FUS portano a una serie di fenotipi patologici quali difetti nello sviluppo neuronale, problemi di locomozione, ridotta sopravvivenza e neurodegenerazione: ad esempio, i topi knockout per il gene FUS mostrano sterilità maschile, difetti nello sviluppo dei linfociti B, aumentata instabilità genomica e vulnerabilità alle radiazioni ionizzanti, mentre in un modello transgenico di *Drosophila* è stato osservato un danno progressivo dei motoneuroni dipendente dall'età quando le varianti FUS WT, R524S o P525L vengono sovraespresse nei neuroni glutamatergici o nei motoneuroni stessi.[10] L'analisi istopatologica dei casi con mutazioni di FUS mostra caratteristiche distintive: le inclusioni risultano positive per FUS, ma negative per TDP-43. Inoltre, nei casi con inclusioni citoplasmatiche neuronali basofile e compatte si osserva un'età di esordio più precoce. [2]

È stato inoltre osservato che le mutazioni localizzate all'estremità C-terminale ne alterano il trasporto nel nucleo, determinandone la localizzazione citoplasmatica e la formazione di SG. La perdita di FUS riduce l'associazione della proteina di riparazione Ku70 ai siti DSB, e il reclutamento di XRCC1/LIG3 agli SSBs, risultando nell'accumulo di lesioni del DNA non riparate. [1, 2]

Aspetti patologici legati a TDP-43

I pazienti con SLA correlata a *TARDBP* presentano generalmente una forma di SLA autosomica dominante con esordio nell'età adulta, con prevalente coinvolgimento degli arti e un'ampia variabilità nell'età di insorgenza (30–77 anni) e nella durata della malattia. [2]

TDP-43 è una proteina legante DNA/RNA appartenente alla famiglia delle ribonucleoproteine. Essa è coinvolta in molteplici funzioni nucleari, tra cui la trascrizione genica, lo splicing dell'RNA, il processamento e la stabilizzazione dei microRNA, nonché il trasporto dell'mRNA. [2]

Quasi tutte le mutazioni su *TARDBP* identificate nei pazienti con SLA sono mutazioni missenso localizzate nella regione C-terminale ricca in glicina, coinvolta nelle interazioni proteina-proteina. TDP-43 possiede numerosi bersagli molecolari, tra cui FUS e altri trascritti che codificano proteine associate a malattie neurodegenerative, oltre a numerosi geni coinvolti nel processamento dell'RNA. [2] La deplezione di TDP-43 ostacola il reclutamento ai DSBs del complesso XRCC4-DNA ligasi IV, che è cruciale per la via di riparazione del DNA non-omologa (NHEJ). [1]

In vivo, l'espressione di TDP-43 umano mutante o wild-type causa una ridotta attività locomotoria e una paralisi progressiva nei topi, e una diminuzione della durata della vita nei moscerini della frutta. [1]

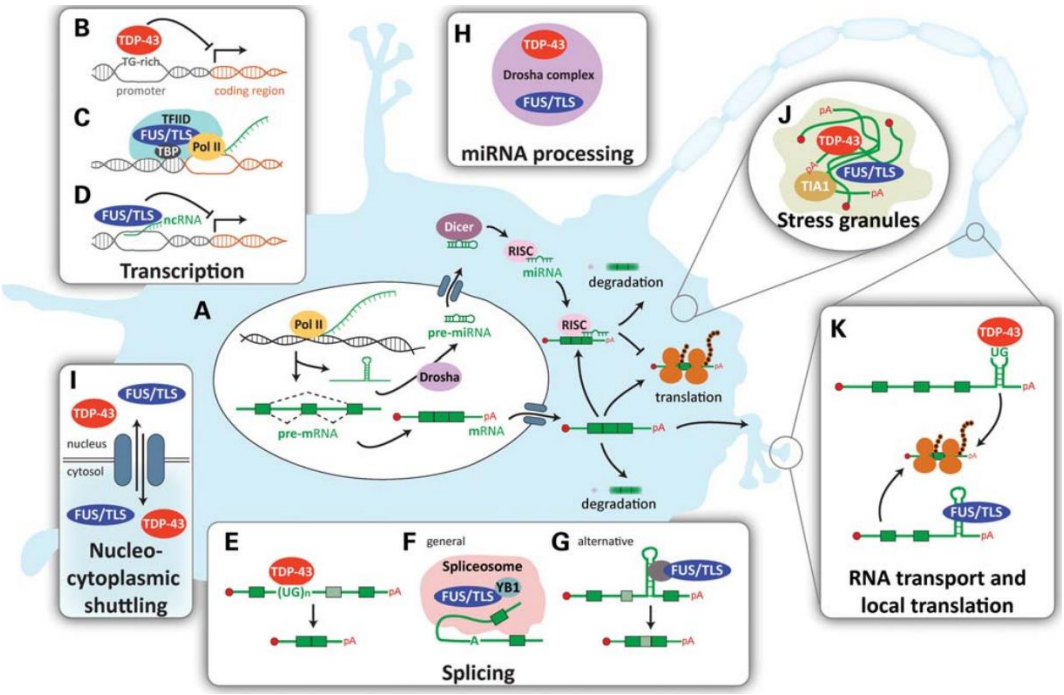

Figura 1: ***Ruoli fisiologici proposti di TDP-43 e FUS/TLS.*** ***(A)*** *Schema riassuntivo delle principali fasi dell'elaborazione dell'RNA, dalla trascrizione alla traduzione o alla degradazione.* ***(B)*** *TDP-43 si lega a elementi ricchi di TG a singolo filamento presenti nelle regioni promotrici, bloccando così la trascrizione del gene a valle.* ***(C)*** *FUS/TLS si associa alla* ***TBP*** *(TATA-binding protein) all'interno del complesso* ***TFIID****, suggerendo che partecipi al macchinario generale della trascrizione.* ***(D)*** *In risposta al danno al DNA, FUS/TLS viene reclutata nella regione promotrice della* ***ciclina D1 (CCND1)*** *da RNA non codificanti (****ncRNA****) senso e antisenso e reprime la trascrizione di* ***CCND1****.* ***(E)*** *TDP-43 si lega a una sequenza continua ricca di* ***UG*** *nelle regioni introniche che precedono esoni soggetti a splicing alternativo, favorendone l'esclusione.* ***(F)*** *FUS/TLS è stata identificata come componente dello* ***spliceosoma*** *e* ***(G)*** *è stato dimostrato che promuove l'inclusione di esoni nell'mRNA di* ***H-ras****, attraverso un legame indiretto con elementi regolatori strutturali localizzati nell'introne a valle.* ***(H)*** *Entrambe le proteine sono state identificate in un complesso con* ***Drosha****, suggerendo un loro possibile coinvolgimento nella maturazione dei* ***miRNA****.* ***(I)*** *Sia TDP-43 sia FUS/TLS sono proteine che traslocano tra il nucleo e il citosol e* ***(J)*** *vengono reclutate nei* ***granuli da stress****, dove formano complessi con mRNA e altre proteine leganti l'RNA.* ***(K)*** *TDP-43 e FUS/TLS sono entrambe coinvolte nel trasporto degli mRNA verso le* ***spine dendritiche*** *e/o il* ***terminale assonale****, dove possono facilitare la traduzione locale. (Immagine presa da: PMID: 20400460)*

METODI UTILIZZATI

Linee cellulari

Le cellule utilizzate sono della linea HeLa, ovvero cellule umane derivanti da un tumore alla cervice uterina, motivo per cui crescono e si duplicano molto più velocemente della media, sono utili per effettuare test sui farmaci.
Le cellule FUCCI-HeLa esprimo il sistema FUCCI (Fluorescent Ubiquitination-based Cell Cycle Indicator) che permette di visualizzare in tempo reale lo stadio del ciclo cellulare tramite l'emissione di specifici colori fluorescenti. Le cellule I-HeLa11 sono una variante geneticamente modificata della classica linea e permettono di tracciare in modo sito-specifico le DSB.
La linea cellulare neuronale HT-22 è un clone immortalizzato derivato dalle cellule HT4 dell'ippocampo di topo.
Le cellule SH-SY5Y, invece, sono una linea cellulare umana derivante da un neuroblastoma, un tumore infantile del sistema nervoso.
Le cellule hMNPs sono linee cellulari di progenitori umani di motoneuroni. Sono state ottenute da iPSCs di controllo e SLA sporadica appaiate per sesso ed età.
In particolare, le hNSCs coltivate in condizioni di adesione sono state differenziate in hMNPs in 7 giorni utilizzando un mezzo composto da 2× Neurobasal, 2× Advanced DMEM/F12, 50× Neural Induction Supplement, 0,1 µM Acido Retinoico e 0,5 µM Purmorfamina. [1, 3]

Colture cellulari e trattamenti

Le cellule FUCCI-HeLa e HT-22 sono state coltivate in terreno DMEM (Dulbecco's Modified Eagle Medium, terreno liquido) contenente 10% FBS, 1% L-glutammina e 1% penicillina/streptomicina (P/S).
Le cellule SH-SY5Y sono state coltivate in DMEM/F12 integrato con 15% FBS e 1% P/S.
Il danno al DNA è stato indotto trattando le cellule con 50 ng/mL di neocarzinostatina per 20 min a 37 °C.
La formazione di granuli da stress è stata indotta trattando le cellule HeLa con 500 µM di arsenito di sodio ($NaAsO_2$) per 30 min a 37 °C.
Le cellule I-HeLa111 sono state coltivate in terreno DMEM integrato con 10% FBS privo di tetraciclina, 1% L-glutammina e 1% P/S e selezionate regolarmente con G418 (1 mg/ml) e igromicina B (300 µg/ml).
Nelle I-HeLa111, le rotture a doppio filamento mediate da I-SceI sono state generate tramite somministrazione di doxiciclina (1 µg/ml) per almeno 16 h.
Per inibire ATM e ATR, le cellule sono state trattate rispettivamente con 5 µM KU60019 e 10 µM VE-821 durante la notte. [1]

Trasfezione

Per ogni plasmide utilizzato, 1–2 µg sono stati trasfettati per 24 h utilizzando Lipofectamine 2000 seguendo le istruzioni del produttore.
Sono stati utilizzati i seguenti plasmidi: pcDNA3.1+ utilizzato come controllo negativo; vettore esprimente TDP-43 WT marcato con MYC; plasmidi esprimenti FUS WT e FUSP525L marcati con FLAG.
Per gli esperimenti di Complementazione di Fluorescenza Bimolecolare, WT FUS o FUSP525L sono stati clonati in pCS2plus-mCerulean 156-239-GGGS e pCS2plus-mVenus1-155-GGGS, utilizzando il kit Gibson Assembly. Per ciascun vettore 0,7 µg sono stati trasfettati utilizzando Lipofectamine 2000. [1]

Immunofluorescenza e analisi delle immagini

L'immunofluorescenza (IF) per TDP-43 e FUS è stata condotta con anticorpi diretti contro le proteine endogene. Le immagini sono state acquisite utilizzando un microscopio confocale a scansione laser lineare.
Le analisi quantitative di immunofluorescenza sono state eseguite in parallelo con parametri di acquisizione e tempi di esposizione identici tra le condizioni.
Per distinguere tra cellule con o senza CIs, a ciascun nucleo cellulare in ogni immagine è stato assegnato un numero univoco con CellProfiler.
È stato calcolato il coefficiente di sovrapposizione di Manders (MOC), che rappresenta la frazione di segnali TDP-43 o FUS sovrapposti a segnali TIA-1 o G3BP1. La soglia inferiore ottimale è stata determinata utilizzando lo strumento di soglia e ispezionata visivamente. È stato considerato il MOC di almeno due repliche biologiche ed effettuato almeno 15 acquisizioni per campione per replica. [1]

Immunoblotting

Le cellule sono state lisate in un tampone Laemmli [2% SDS, 5% glicerolo, 1,5% ditiotreitolo (DTT), 0,01% Blu di bromofenolo e 60 mM Tris-HCl pH 6,8] e sono state successivamente sottoposte a sonicazione e riscaldate per 10 min a 95°C. Sono stati caricati 10–15 µl di lisato su un gel di SDS–poliacrilammide. È stata poi applicata una tensione di 60 V per la prima fase di stacking e di 150 V per la successiva di separazione. I gel sono stati fatti correre in tampone per elettroforesi di Tris-glicina (25 mM Tris, 250 mM glicina e 0,1% SDS).
Per l'analisi mediante western blot, le proteine sono state trasferite su una membrana di nitrocellulosa da 0,2 µm. Il trasferimento è stato eseguito a 25 V per 7 o 10 min (in base al peso molecolare delle proteine analizzate). Le membrane sono state incubate con latte scremato al 5% in tampone TBS-T (TBS contenente 0,1% Tween-20) per 1 h, seguite da incubazione overnight a 4°C con l'anticorpo primario e tre lavaggi con TBS-T prima di un'incubazione di 1 h a temperatura ambiente con il corrispondente anticorpo secondario coniugato a HRP.

La rilevazione chemiluminescente è stata effettuata mediante incubazione con Luminata Classico o Crescendo. Le proteine sono state visualizzate tramite autoradiografia su pellicole ECL utilizzando diversi tempi di esposizione e sviluppo manuale, oppure mediante un sistema di imaging Chemidoc. [1]

Comet assay

Il comet assay permette di misurare il danno al DNA nelle singole cellule. Il test sfrutta l'elettroforesi su gel in cui il DNA frammentato crea delle bande più piccole che migrano quindi più velocemente verso il polo positivo; maggiore è il danno e più lunga e luminosa sarà la "coda" della "cometa".
Le cellule HeLa sono state tripsinizzate, lavate una volta con PBS ghiacciato e risospese in PBS freddo alla concentrazione finale di 10^5 cellule ml^{-1}. La sospensione cellulare è stata quindi mescolata con agarosio a basso punto di fusione preriscaldato in rapporto 1:10 (v/v) e distribuita sui vetrini.
La lisi è stata effettuata overnight a 4 °C. L'elettroforesi è stata condotta in tampone di elettroforesi neutro per 45 min a 21 V. Dopo la precipitazione del DNA e il lavaggio in etanolo al 70%, i vetrini sono stati asciugati e il DNA colorato con SYBR Gold prima dell'analisi mediante microscopia a epifluorescenza. Il "comet tail moment" è stato calcolato utilizzando il software OpenComet. [1]

BrdU incorporation assay

Questa tecnica permette di misurare la proliferazione cellulare e di identificare le cellule che si stanno dividendo attivamente, per fare ciò, si sfrutta l'analogia chimica tra la bromodeossiuridina e la timina.
Dopo la trasfezione del plasmide, le cellule sono state trattate con 10 µM BrdU e incubate a 37 °C per una notte. Il giorno successivo, le cellule sono state lavate due volte in PBS e fissate in paraformaldeide al 4% per 10 min a temperatura ambiente. I vetrini sono stati poi lavati due volte in PBS e bloccati in PBG (0,5% di albumina sierica bovina, 0,2% di gelatina da pelle di pesce d'acqua fredda) per 1 ora a temperatura ambiente. Successivamente, i vetrini sono stati incubati per un'ora a temperatura ambiente in una camera umida con una miscela PBG contenente un anticorpo primario anti-BrdU diluito 1:20, di RQ1 DNAsi e buffer di RQ1 DNAsi, ciascuno diluito 1:10. Dopo l'incubazione con l'anticorpo primario, le cellule sono state lavate tre volte in PBS ed è stata eseguita l'immunofluorescenza. [1]

EU incorporation assay

Gli RNA sono stati marcati mediante un impulso di 1 ora con 5-EU 1 mM. Le cellule sono state quindi fissate in paraformaldeide al 4% e i livelli di incorporazione di EU sono stati rilevati utilizzando il kit Click-iT per l'imaging dell'RNA secondo le istruzioni del produttore. [1]

Cell sorting

A 24 h dalla trasfezione, le cellule sono state lavate due volte con PBS, delicatamente raschiate e raccolte in 1 mL di tampone di sorting (2 mM EDTA, 20 mM HEPES pH 7,3 in PBS 1X) per ciascuna condizione, trasferite in provette da 15 mL e mantenute in ghiaccio. Successivamente, i campioni sono stati trasferiti in Falcon da 5 mL dotati di filtro in nylon da 35 μm e vortexati accuratamente per dissociare eventuali aggregati cellulari formatisi.

Per impostare i gate, sono state inizialmente analizzate 30 000 cellule trasfettate con il vettore vuoto tramite un S3e Cell sorter (Bio-Rad). Successivamente, le cellule esprimenti WT o FUS^{P525L} sono state separate in modalità purity (permette di massimizzare l'accuratezza e la purezza della popolazione cellulare separata) e le cellule positive sono state raccolte.

Dopo il sorting cellulare, le cellule sono state centrifugate a 4°C per 1,5 min alla massima velocità e il surnatante è stato eliminato. Le cellule sono state quindi lisate per l'estrazione dell'RNA oppure congelate a −80°C per utilizzi successivi. [1]

qRT-PCR

L'estrazione di RNA è stata eseguita utilizzando il kit miRNeasy Mini, secondo le istruzioni del produttore. Successivamente, 1 μg di RNA totale è stato retrotrascritto utilizzando il sistema SuperScript IV First-Strand Synthesis. Per il rilevamento del dilncRNA nelle cellule I-HeLa111, 500 ng di RNA totale sono stati retrotrascritti con il sistema SuperScript III First-Strand Synthesis utilizzando primer specifici per il gene. I campioni sono stati poi raffreddati su ghiaccio e incubati per 20 min a 37 °C con 1 μL di RNasi H. [1]

Motoneuroni murini

Le cellule coltivate per 2 giorni dopo la dissociazione dei corpi embrioidi sono state ripiastrate su vetrini di vetro prelavati e pretrattati con HCl 1 M (0,01% poli-L-ornitina, 20 mg/mL laminina) e fissate in PBS contenente 4% PFA, 4% saccarosio e 5 mM $MgCl_2$ per 30 min a 4 °C. Le cellule sono state poi lavate una volta in PBS contenente 2% saccarosio e poi due volte in PBS contenente 4% saccarosio. Dopo i passaggi di disidratazione con etanolo a temperatura ambiente (50%, 70%), le cellule sono state conservate a +4 °C in etanolo assoluto + 1:100 VRC. Le cellule sono state poi permeabilizzate con 0,2% (0,25% per p53BP1 IF) Triton X-100 per 20 min a temperatura ambiente, bloccate in 1% siero di capra/1% siero di asino (2% BSA per p53BP1 IF)/PBS per 1 h e poi incubate con anticorpi primari anti-γH2AX, anti-fosfo-53BP1, anti-DROSHA o anti-TLS/FUS policlonale di coniglio e anti-beta III tubulina durante la notte a 4 °C. Successivamente, sono state incubate con anticorpi secondari donkey anti-rabbit Alexa Fluor Plus 647 e goat anti-chicken Alexa 488 diluiti 1:200 in 1% siero di capra/1% siero di asino (2% BSA per p53BP1

IF)/PBS per 45 min a temperatura ambiente. Dopo due lavaggi in PBS, le cellule sono state incubate con soluzione DAPI per 5 min a temperatura ambiente e poi montate usando ProLong Diamond Antifade Mountant. [1]

Immunoistochimica

L'immunoistochimica (IHC) sfrutta la reazione chimica altamente specifica tra un anticorpo e un antigene bersaglio per localizzare e visualizzare proteine o altre macromolecole direttamente all'interno delle sezioni di un tessuto biologico, il principio è quindi analogo a quello dell'immunoblotting, con la differenza che gli anticorpi vengono incubati in sottili sezioni di tessuto o monostrati di cellule in coltura, adesi e fissati su vetrino.
Quindi per ogni sezione studiata, cinque campi non sovrapposti sono stati analizzati utilizzando l'algoritmo di segmentazione Multiplex IHC. [1]

Ceppi di *Drosophila*

I ceppi di *Drosophila* e gli incroci sono stati mantenuti su terreno standard (Nutri-fly, Genesee Scientific) a 25 °C. La linea transgenica UAS-hTDP-43 è stata fornita da Fabian Feiguin, mentre Bloomington Drosophila Stock Center ha fornito il driver GAL4 e gli altri ceppi utilizzati: eyeless-GAL4, inserito sul secondo cromosoma; entrambi i transgeni Dicer erano inseriti sul terzo cromosoma. [1]

Analisi degli occhi di *Drosophila melanogaster*

Le immagini degli occhi delle mosche sono state acquisite utilizzando uno stereomicroscopio (ZEISS Stemi 508, 50×) equipaggiato con una fotocamera Axiocam 105 e il software ZEISS ZEN (edizione Blue). L'area dell'occhio è stata misurata mediante il software open source NIH ImageJ FIJI. [1]

Marcatura dei dischi immaginali oculari di *Drosophila*

I cervelli larvali sono stati isolati afferrando gli uncini boccali con un paio di pinzette e tirando delicatamente il resto del corpo con un secondo paio di pinzette, in una goccia di tampone fisiologico salino. I dischi immaginali oculari e antennali rimanevano attaccati al cervello tramite gli uncini boccali, che venivano utilizzati per trasferire i campioni nel mezzo di fissazione.
I tessuti larvali sono stati fissati per 1 ora in tampone di fissazione (4% paraformaldeide, 4% saccarosio in tampone fosfato), permeabilizzati con 0,25% Triton X-100 in PBS e successivamente incubati in soluzione di blocco (0,1% Triton X-100, 3% BSA in PBS).
Sono stati utilizzati i seguenti anticorpi: anticorpo anti-fosfo-Istone H3 (Ser10) (Merck), diluito 1:500 e incubato overnight; anticorpo secondario donkey anti-rabbit Oregon Green (Jackson ImmunoResearch), diluito 1:300.

L'analisi in immunofluorescenza è stata eseguita utilizzando un microscopio a epifluorescenza Axiophot (Carl Zeiss), mentre le immagini di fluorescenza sono state elaborate con Adobe Photoshop. [1]

Analisi statistica

Non sono stati utilizzati criteri per determinare la dimensione del campione, ma sono stati raccolti quanti più dati possibile a seconda della natura degli esperimenti o per avere un'analisi statistica. Per gli studi sugli animali, non sono stati utilizzati metodi statistici per stimare la dimensione del campione.

Per ogni esperimento, sono stati eseguiti almeno tre replicati biologici, salvo indicazioni contrarie.

Per gli esperimenti in vitro, i pozzetti sono stati assegnati casualmente a ciascun gruppo e tutte le cellule sono state analizzate in modo uguale

Per esperimenti in vivo su topi, gli animali sono stati assegnati in modo casuale ai gruppi sperimentali. Nessun metodo blind è stato applicato, poiché è stato utilizzato un software imparziale per la raccolta e l'analisi dei dati. Il software Prism 9 è stato usato per generare grafici, eseguire analisi statistiche e occasionalmente rimuovere valori con il metodo di regressione robusta e rimozione degli outlier. L'analisi statistica è stata eseguita utilizzando l'ANOVA a una via, assumendo SD uguali tra i gruppi analizzati; è stato applicato un t-test a due code non appaiato. [1]

RISULTATI

La formazione di inclusioni citoplasmatiche di TDP-43 e della proteina FUS mutante è associata all'accumulo di danni al DNA

Per indurre la formazione di CIs, cellule HeLa sono state transientemente trasfettate con plasmidi esprimenti FUS o TDP-43 di tipo wild-type e le loro forme mutanti associate alla SLA: FUS^{P525L}, TDP-43^{A382T} e TDP-43^{I383V}, in parallelo a un vettore vuoto (EV) come controllo. Le analisi di Western blot hanno confermato che le quantità delle proteine risultavano comparabili ai rispettivi livelli endogeni.

Successivamente, tramite immunofluorescenza, utilizzando anticorpi contro le proteine endogene, è stata vista la localizzazione subcellulare di FUS e TDP-43. In particolare, si è osservata la loro segregazione in CIs in circa il 30% e il 15–20% delle cellule che sovraesprimevano FUS^{P525L} e TDP-43, rispettivamente. Al contrario, la frazione di cellule che mostravano CIs positivi per TDP-43 endogena era meno del 3% nei campioni trasfettati con EV, a indicare che soltanto il mutante FUS patologico forma CIs. Al contrario, le mutazioni di TDP-43 non aumentavano la tendenza della proteina a formare CIs. La maggior parte delle CIs di FUS^{P525L} e TDP-43 è stata osservata colocalizzare con i SGs.

Sono stati analizzati gli effetti della formazione di CIs sull'accumulo di danni al DNA, trattando cellule che esprimevano FUS o TDP-43 con Neocarzinostatina (NCS), un farmaco utilizzato per generare DSB, seguito da analisi tramite IF. Si è visto che la localizzazione di FUS^{P525L} o TDP-43 nelle CIs non era influenzata dal trattamento con NCS, indicando che il danno al DNA è una conseguenza dell'aggregazione di FUS^{P525L} o TDP-43. (Fig. 2A, B)

Al contrario di quanto osservato nelle cellule con Cls di FUS mutante e TDP-43, le cellule trasfettate con FUS WT o con EV mostravano un basso livello di danno endogeno al DNA e formavano correttamente foci di DDR positivi alla γH2AX dopo trattamento con NCS. [1] (Fig. 2C, D)

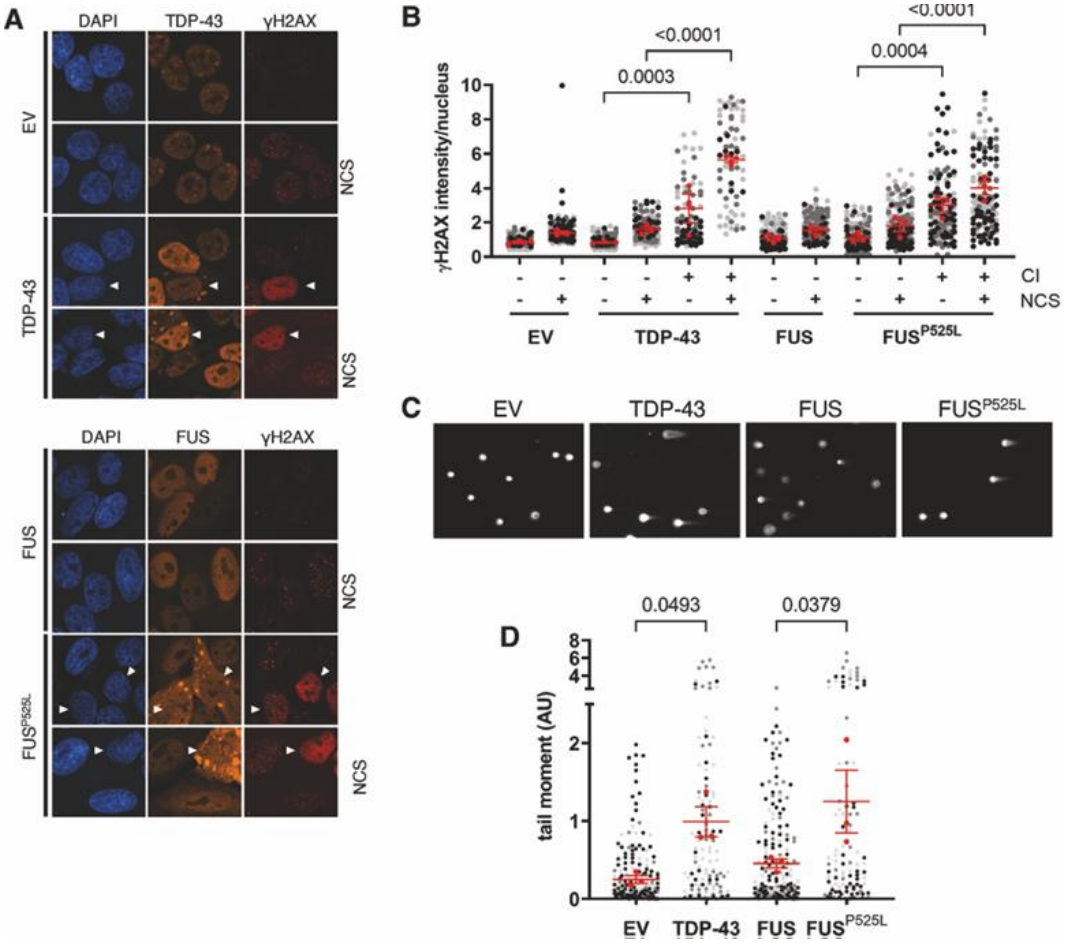

Figura 2: ***Le cellule contenenti inclusioni citoplasmatiche (CI) di TDP-43 o FUS^P525L^ mostrano livelli elevati di γH2AX e un aumento della formazione di rotture a doppio filamento del DNA (DSB). A*** *Analisi mediante immunofluorescenza (IF) del segnale di γH2AX (rosso) in cellule HeLa danneggiate (NCS) o non danneggiate, trasfettate con plasmidi che esprimono TDP-43, FUS o FUS^P525L^. Le cellule trasfettate con un vettore vuoto (EV) sono state utilizzate come controllo. I segnali di TDP-43 e FUS sono visualizzati in arancione; i nuclei sono stati controcolorati con DAPI (blu). Le punte di freccia indicano le cellule contenenti inclusioni citoplasmatiche (CI).* ***B*** *Super-plot che mostra la quantificazione dell'intensità del segnale di γH2AX nelle cellule HeLa con o senza inclusioni citoplasmatiche (± CI), determinata come mostrato nel pannello* ***(A)****. I punti rossi rappresentano i valori medi di ciascuna replica biologica; le barre rosse indicano la media ± errore standard della media (SEM) di tre esperimenti indipendenti.* **C** Immagini rappresentative di esperimenti di **comet assay** eseguiti su cellule HeLa non danneggiate, trasfettate come descritto nel pannello **(A)**. **D** Analisi del **tail moment** nelle cellule HeLa mostrate nel pannello **(C)**. I punti rossi dei super-plot rappresentano i valori medi di ciascuna replica biologica; le barre rosse indicano la media ± errore standard della media (SEM) di tre esperimenti indipendenti

ATM è iperattivata ed è responsabile dell'aumento dei livelli di γH2AX nelle cellule con inclusioni citoplasmatiche.

Uno studio precedente aveva mostrato un accumulo di γH2AX pan-nucleare in risposta all'attivazione di ATM in differenti contesti di alterazione della struttura

della cromatina. Al contrario, l'attivazione di ATR è stata occasionalmente associata a un segnale γH2AX pan-nucleare durante lo stress replicativo.
Per determinare quindi quale chinasi fosse responsabile dell'accumulo di γH2AX, cellule che esprimevano FUS^{P525L}, TDP-43 o campioni di controllo sono state trattate con inibitori specifici dell'attività chinasica di ATM o ATR ed è stato monitorato il loro impatto sui segnali γH2AX mediante immunofluorescenza.
L'inibizione di ATM ha quasi completamente abolito il segnale γH2AX nelle cellule con CIs di TDP-43 o FUS^{P525L}, rispetto ai campioni di controllo trattati con il veicolo. D'altra parte, l'inattivazione di ATR ha ridotto solo marginalmente il segnale γH2AX in cellule con CIs di TDP-43. [9] (Fig. 3A, B) È stato inoltre osservato che le cellule non trattate con NCS e contenenti CIs di TDP-43 o FUS^{P525L} mostravano un segnale corrispondente a pATM anormalmente diffuso, in contrasto con quelle che esprimevano TDP-43 o FUS^{P525L} ma prive di Cis, suggerendo che la formazione di CIs sia sufficiente a innescare un'attivazione diffusa e aberrante di ATM anche in assenza di induzione di danno al DNA. (Fig. 3C, D) Nel complesso, i risultati indicano che l'accumulo di γH2AX pan-nucleare dipende da un'attivazione disfunzionale di ATM, responsabile dei livelli pan-nucleari di γH2AX ma incapace di trasmettere efficacemente il segnale della DDR alle chinasi effettrici a valle. (Fig. 3A, B)
Per confermare questa ipotesi, sono state utilizzate cellule HeLa, esprimenti il sistema FUCCI, trasfettate con plasmidi che esprimevano TDP-43, FUS, FUS^{P525L}, oppure un vettore vuoto come controllo. La grande maggioranza delle cellule con CIs di TDP-43 e FUS^{P525L} (rispettivamente 96% e 91%) era positiva per G1. Al contrario, solo il 60–70% delle cellule prive di CIs oppure esprimenti FUS wild-type o EV risultava positivo per G1. [1]

Le inclusioni citoplasmatiche di FUS^{P525L} e TDP-43 ostacolano la formazione ed il reclutamento di 53BP1 ai DSB

Nelle cellule con CIs, il trattamento con NCS non è risultato in grado di indurre la normale formazione dei foci di 53BP1, indicando un difetto nel suo reclutamento ai siti di danno. Inoltre, anche la fosforilazione di 53BP1 è risultata significativamente ridotta, pur in presenza di livelli normali della proteina totale, suggerendo che le CIs interferiscano con la sua attivazione e non con la sua espressione. (Fig. 3C, D, E)
È stata quindi analizzata MDC1, una proteina coinvolta nelle fasi iniziali della DDR e nel reclutamento di 53BP1. A differenza di 53BP1, MDC1 è stata osservata formare normalmente foci nei siti di danno anche nelle cellule contenenti CIs di FUS^{P525L} o TDP-43. Questi risultati indicano quindi che le inclusioni citoplasmatiche compromettono selettivamente alcune fasi della DDR, bloccando la trasduzione del segnale verso 53BP1 senza alterare il reclutamento di MDC1.

Infine, per verificare se i soli SGs fossero responsabili di questi difetti, le cellule sono state trattate con arsenito di sodio per indurne la formazione. Sebbene quasi tutte le cellule sviluppassero SGs, non è stato osservato né accumulo di danno al DNA né alterazioni nella risposta DDR: le cellule trattate sono risultate infatti ancora capaci di formare correttamente foci di 53BP1 dopo danno indotto. [1]

La trascrizione è repressa nelle cellule con inclusioni citoplasmatiche di TDP-43 o FUS^{P525L}

Per capire se i livelli di danno al DNA aumentati osservati nelle cellule con CIs di TDP-43 e FUS fossero correlati anche a un'inibizione della trascrizione, è stata monitorata la trascrizione de novo nelle cellule con CIs, marcando gli RNA neosintetizzati in colture cellulari esprimenti TDP-43 e FUS^{P525L} con 5-etieniluridina (EU), seguita da analisi mediante microscopia a fluorescenza. (Fig. 4A, B) È stato osservato un segnale di incorporazione di EU significativamente ridotto nelle cellule con CIs sia di TDP-43 sia di FUS^{P525L}, indicando una repressione trascrizionale globale. [1] (Fig. 3A, B)

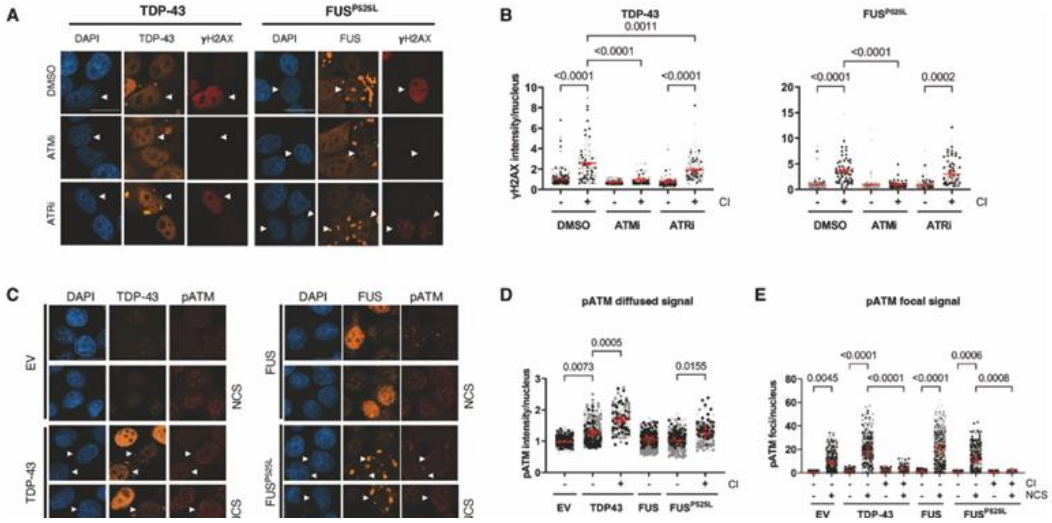

Figura 3: ***ATM è attivata in modo aberrante e la sua inibizione abolisce la formazione pan-nucleare di γH2AX nelle cellule contenenti inclusioni citoplasmatiche (CI) di TDP-43 e FU^{P525L}.*** ***A*** *Analisi mediante immunofluorescenza (IF) dei livelli di γH2AX (rosso) in cellule HeLa che esprimono TDP-43 o FUS^{P525L} e trattate con un inibitore di ATM (ATMi) o un inibitore di ATR (ATRi). Le cellule trattate con DMSO sono state utilizzate come controllo. TDP-43 e FUS sono visualizzate in arancione; i nuclei sono stati colorati con DAPI. Le punte delle frecce indicano le cellule contenenti inclusioni citoplasmatiche (CI); barra di scala = 10 µm.* ***B*** *Quantificazione dell'intensità del segnale di γH2AX nelle cellule HeLa ± CI, come descritto in* ***(A)****. I punti rossi dei super-plot rappresentano i valori medi di ciascuna replica biologica; le barre rosse indicano la media ± errore standard della media (SEM) di tre esperimenti indipendenti.* ***C*** *Analisi mediante immunofluorescenza (IF) del segnale di pATM (rosso) in cellule HeLa trasfettate con plasmidi che esprimono un vettore vuoto (EV), TDP-43 o FUS^{P525L}. TDP-43 e FUS sono visualizzate in arancione; i nuclei sono stati colorati con DAPI. Le punte di freccia indicano le cellule contenenti inclusioni citoplasmatiche (CI); barra di scala = 10 µm.* ***D, E*** *Quantificazione del segnale di pATM diffuso e puntiforme (diffuse e focal), rispettivamente (****D*** *ed* ***E****), nelle cellule HeLa con o senza inclusioni citoplasmatiche (± CI), determinata come mostrato in* ***(C)****. I punti rossi dei super-plot rappresentano i valori medi di ciascuna replica biologica; le barre rosse indicano la media ± errore standard della media (SEM) di tre esperimenti indipendenti.*

La biogenesi degli RNA non codificanti indotti dal danno è difettosa nelle cellule contenenti inclusioni citoplasmatiche

Normalmente, dopo la formazione di rotture a doppio filamento (DSB), l'RNA polimerasi II sintetizza nei siti di danno lunghi RNA non codificanti indotti dal danno (dilncRNA), successivamente processati da DROSHA e DICER in DDRNA, molecole fondamentali per l'attivazione della DDR e la riparazione del DNA. [9] (Fig. 4A, B)

Per studiare questo processo, sono state utilizzate cellule I-HeLa111 con un DSB inducibile tramite la nucleasi I-SceI. I risultati hanno mostrato che le cellule esprimenti FUS wild-type aumentavano correttamente i livelli di dilncRNA dopo il danno al DNA, mentre quelle con FUS^{P525L} non riuscivano a indurne la sintesi. (Fig. 4C)

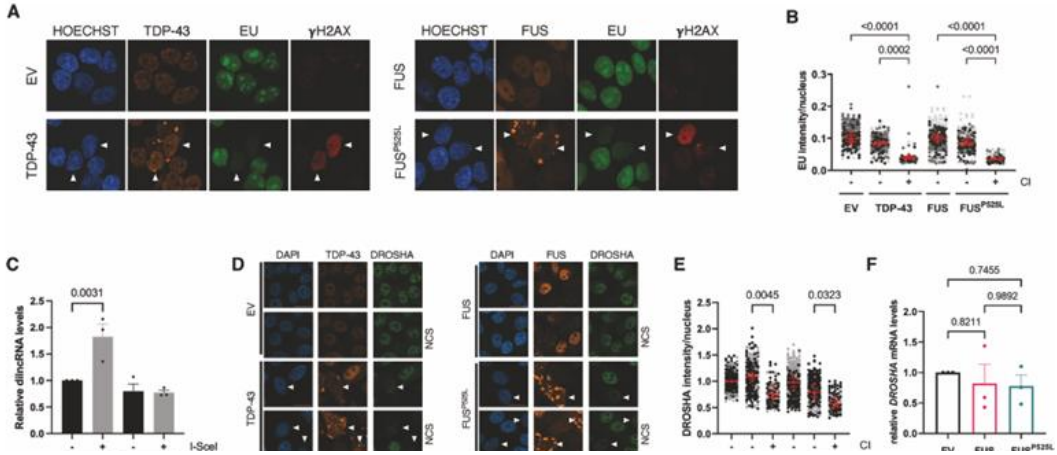

Figura 4: ***La trascrizione è arrestata nelle cellule contenenti inclusioni citoplasmatiche (CI) di TDP-43 e FUS^P525L^.*** ***A*** *Cellule HeLa che esprimono TDP-43, FUS o FUS^P525L^ sono state sottoposte a marcatura a impulso con EU (5-etiniluridina) e successivamente analizzate mediante immunofluorescenza. TDP-43 e FUS, l'EU e γH2AX sono visualizzati rispettivamente in arancione, verde e rosso. Il DNA nucleare è stato visualizzato mediante colorazione con Hoechst; le punte di freccia indicano le cellule contenenti inclusioni citoplasmatiche (CI).* ***B*** *Quantificazione del segnale dell'EU nelle cellule con o senza inclusioni citoplasmatiche (± CI), mostrate nel pannello* ***(A)****. I punti rossi dei super-plot rappresentano i valori medi di ciascuna replica biologica; le barre rosse indicano la media ± errore standard della media (SEM) di tre esperimenti indipendenti.* ***C*** *L'espressione degli RNA lunghi non codificanti indotti dal danno (damage-induced long non-coding RNA,* ***dilncRNA****) è stata analizzata mediante RT-qPCR strand-specifica in cellule I-HeLa111 tagliate (****I-SceI+****) o non tagliate (****I-SceI−****), selezionate mediante FACS per la presenza di inclusioni citoplasmatiche (CI) di FUS o FUS^P525L^. L'istogramma mostra i livelli di dilncRNA normalizzati rispetto all'mRNA di* ***RPLP0*** *ed espressi relativamente al campione non tagliato che esprime FUS; i valori rappresentano la media ± SEM di tre esperimenti indipendenti.****D*** *Immagini rappresentative dell'espressione di DROSHA (verde) in cellule HeLa danneggiate (NCS) o non danneggiate, trasfettate con plasmidi codificanti TDP-43, FUS o FUS^P525L^. Le cellule trasfettate con un vettore vuoto (EV) sono state utilizzate come controllo. TDP-43 e FUS sono visualizzate in arancione; i nuclei sono stati controcolorati con DAPI. Le punte di freccia indicano le cellule contenenti inclusioni citoplasmatiche (CI); barra di scala = 10 µm.* ***E*** *Quantificazione dei livelli della proteina DROSHA nelle cellule con o senza inclusioni citoplasmatiche (± CI) del pannello* ***(D)****. I punti rossi dei super-plot rappresentano i valori medi di ciascuna replica biologica; le barre rosse indicano la media ± errore standard della media (SEM) di tre esperimenti indipendenti.* ***F*** *I livelli di mRNA di* ***DROSHA*** *sono stati monitorati mediante RT-qPCR in cellule HeLa selezionate mediante FACS per la presenza di inclusioni citoplasmatiche (CI) di FUS o FUS^P525L^. I valori rappresentano la media ± SEM di tre esperimenti indipendenti.*

Inoltre, le cellule con inclusioni di TDP-43 o FUS^{P525L} presentavano una riduzione dei livelli proteici di DROSHA, senza però variazioni dell'mRNA corrispondente, suggerendo che l'aggregazione proteica possa compromettere la stabilità di DROSHA a livello post-traduzionale. Al contrario, i livelli di DICER non hanno mostrato variazioni significative. [1] (Fig. 4D, E, F)

Le aggregazioni citoplasmatiche di TDP-43 e FUS sono correlate a una DDR difettosa, accumulo di danno al DNA e ridotti livelli di DROSHA in linee neuronali

Lo studio ha analizzato poi gli effetti delle CIs di TDP-43 e FUS in diverse linee cellulari neuronali, per verificare se alterassero la DDR, come già osservato nelle cellule HeLa. Nelle cellule di neuroblastoma umano SH-SY5Y, TDP-43 è risultata indurre la formazione di inclusioni associate ai GS, al contrario di FUS^{P525L}. Le cellule con CIs di TDP-43 hanno mostrato inoltre un aumento del danno al DNA (γH2AX), un ridotto reclutamento di 53BP1 dopo trattamento con NCS ed una diminuzione della ciclina A, indicando alterazioni della DDR e della progressione del ciclo cellulare. [5] Risultati simili sono stati ottenuti nelle cellule neuronali ippocampali murine HT-22: le inclusioni di TDP-43 e FUS^{P525L} hanno causato un aumento di γH2AX e una riduzione dei foci di 53BP1. Tuttavia, non è stata osservata attivazione di p53 fosforilata, suggerendo che le inclusioni non attivino questa via di risposta cellulare. Gli esperimenti sono stati poi estesi a progenitori di motoneuroni umani derivati da iPSC di pazienti con SLA sporadica e a motoneuroni murini maturi con mutazione FUS^{P517L}. In entrambe le cellule si sono osservate alterazioni tipiche: delocalizzazione citoplasmatica di TDP-43 o FUS, aumento del danno al DNA, riduzione di 53BP1 e diminuzione dei livelli di DROSHA.
Nel complesso, i risultati hanno dimostrato che l'alterata distribuzione subcellulare di TDP-43 e FUS nelle cellule neuronali compromette la risposta al danno del DNA, favorisce l'accumulo di danni genomici e riduce l'espressione di DROSHA. [1, 4]

L'enoxacina stimola la DDR e riduce l'accumulo di danni al DNA in un modello murino di SLA associato a FUS

L'enoxacina, un antibiotico fuorochinolonico, è in grado di potenziare l'attività enzimatica di DICER. È stato infatti dimostrato che il trattamento con enoxacina promuove la biogenesi degli RNA brevi DICER-dipendenti e stimola la segnalazione della DDR e la riparazione del DNA in cellule in coltura. [1]
Per valutare se questo effetto possa essere rilevante anche nel contesto della patologia associata a FUS, è stata somministrata enoxacina a topi non patologici (eterozigoti) o patologici (omozigoti) che sovraesprimono l'omologo umano wild-type di FUS (hFUS). Successivamente è stata analizzata l'attivazione della DDR e

l'accumulo di danni effettuando una colorazione del midollo spinale murino per γH2AX e 53BP1 tramite la tecnica di immunoistochimica (IHC).
In linea con i risultati delle cellule in coltura, i topi omozigoti hFUS hanno mostrato livelli più elevati di γH2AX nel midollo spinale e segnali ridotti di 53BP1 rispetto agli animali eterozigoti. (Fig. 5A, B) Inoltre, nei topi omozigoti trattati con enoxacina è stato osservato un aumentato segnale di 53BP1, con, al contrario, ridotti livelli di γH2AX rispetto agli animali trattati con il solo veicolo.
Nel loro insieme, questi risultati suggeriscono che la somministrazione in vivo di enoxacina in topi con patologia FUS è efficace nello stimolare la DDR e nel ridurre l'accumulo di danni al DNA. [1] (Fig. 5A, B)

La sovraespressione di DICER contrasta la neurodegenerazione in un modello di SLA di *Drosophila melanogaster*

Per capire come la somministrazione di enoxacina possa influire sulla neurodegenerazione è stato utilizzato un modello di *Drosophila melanogaster* di neurotossicità mediata da TDP-43, in cui l'espressione ectopica della proteina TDP-43 umana (hTDP-43) causa una degenerazione retinica progressiva, come mostrato da una significativa riduzione dell'area oculare. (Fig. 5C, D)
Diversamente dai mammiferi, il genoma di *D. melanogaster* codifica per due distinti enzimi DICER: DICER-1, coinvolto principalmente nella biogenesi citoplasmatica dei miRNA, e DICER-2, con un ruolo più rilevante nel processamento dei siRNA nel nucleo. Di conseguenza, per imitare gli effetti della somministrazione di enoxacina in questo sistema, sono state sovraespresse entrambe le isoforme di DICER in mosche esprimenti hTDP-43 ed è stato monitorato il loro impatto sulla degenerazione retinica. (Fig. 5C, D) A differenza di quanto ci si aspettasse, la sovraespressione di DICER-2 ha permesso di recuperare significativamente l'area oculare nelle mosche esprimenti hTDP-43. Al contrario, non sono stati osservati effetti rilevanti nelle mosche esprimenti hTDP-43 e DICER-1, escludendo un ruolo centrale per i miRNA nel prevenire la degenerazione retinica. (Fig. 5C, D)
Questi risultati indicano che stimolare le funzioni di DICER può essere utile nel contrastare la neurodegenerazione mediata da TDP-43. [1]

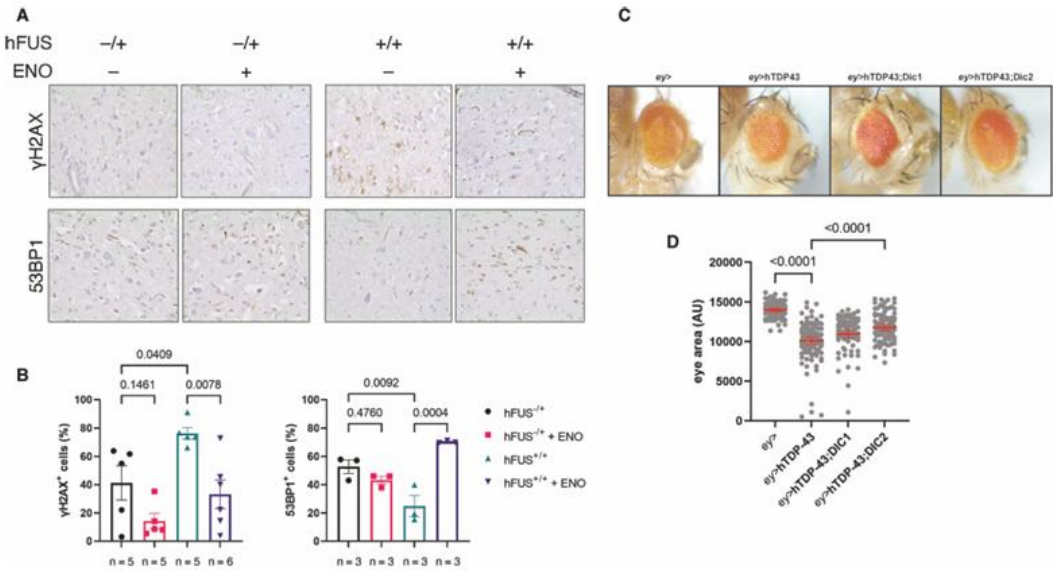

Figura 5: **L'enoxacina stimola la risposta al danno del DNA (DDR) e riduce l'accumulo di danni al DNA nel midollo spinale di topi che esprimono hFUS. La sovraespressione di Dicer-2 contrasta la degenerazione della retina negli occhi di Drosophila melanogaster che esprimono hTDP-43 A** Immagini rappresentative di immunoistochimica (IHC) di sezioni di midollo spinale di topi che esprimono hFUS, trattati con enoxacina o con il veicolo di controllo e colorati per γH2AX e 53BP1. **B** Quantificazione della percentuale di cellule positive per i marcatori indicati, determinata come mostrato nel pannello **(A)**. I valori rappresentano la media ± errore standard della media (SEM). Per ciascuna condizione sono stati analizzati almeno tre topi; il numero esatto è riportato sotto ciascun istogramma. **C** Immagini rappresentative degli occhi di Drosophila melanogaster adulte che esprimono i costrutti indicati sotto il controllo del promotore **eyeless-GAL4**. ***D*** *Grafico a punti (dot plot) che mostra la quantificazione dell'area media dell'occhio nelle mosche con i genotipi indicati; sono stati analizzati oltre 70 occhi per ciascun genotipo in tre esperimenti indipendenti. Le barre rosse rappresentano la media ± errore standard della media (SEM).*

CONCLUSIONI E DISCUSSIONE

La SLA è caratterizzata dall'accumulo di CIs insolubili contenenti TDP-43 e FUS, proteine che, in condizioni fisiologiche, svolgono un ruolo fondamentale nel mantenimento della stabilità genomica partecipando ai processi di riparazione del danno al DNA. FUS viene reclutata nei siti di lesione attraverso l'interazione con le catene di poli(ADP-ribosio) (PAR) e promuove il reclutamento del complesso di riparazione XRCC1/LIG3, mentre TDP-43 contribuisce alla riparazione delle DSB mediante la via di giunzione delle estremità non omologhe (NHEJ). La perdita della funzione di queste proteine è stata quindi correlata a instabilità genomica e ridotta sopravvivenza neuronale. [1, 5] (Fig. 3C, D, E)

Recenti evidenze hanno dimostrato che la formazione di inclusioni citoplasmatiche di TDP-43 e della variante mutata FUS^{P525L}, associate ai SGs, altera la DDR determinando un accumulo di DSB. Le cellule contenenti tali inclusioni presentano un'iperattivazione della chinasi ATM e un marcato incremento del segnale di γH2AX, indicativo di un danno genomico persistente. Inoltre, nelle cellule con inclusioni di TDP-43, anche ATR sembra contribuire, seppur in misura minore, all'attivazione della risposta al danno, probabilmente in conseguenza dei difetti di replicazione del DNA associati alla disfunzione di questa proteina. [1] (Fig. 2, 3)

L'alterazione della DDR determina anche una compromissione della trascrizione globale. L'attivazione aberrante di ATM induce infatti modificazioni della cromatina che ostacolano l'attività della RNA polimerasi II, mentre la perdita di funzione di TDP-43 e FUS favorisce l'accumulo di danni al DNA nei siti di trascrizione attiva. Tale difetto trascrizionale assume particolare rilevanza nei neuroni, caratterizzati da trascritti mediamente più lunghi e quindi maggiormente suscettibili agli effetti dell'inibizione della trascrizione, contribuendo alla maggiore vulnerabilità del tessuto nervoso nella SLA. [6] (Fig. 6)

La presenza di aggregati citoplasmatici compromette inoltre la biogenesi degli RNA coinvolti nella DDR. Oltre a ridurre la sintesi degli RNA non codificanti indotti dal danno, gli aggregati determinano una diminuzione dei livelli nucleari di DROSHA interferendo con l'efficienza dei meccanismi di riparazione. Questo fenomeno può instaurare un circolo vizioso che favorisce il progressivo accumulo di lesioni genomiche. [9] (Fig. 4C, D, E)

Infine, è stato dimostrato che il potenziamento dell'attività di DICER mediante enoxacina ripristina una DDR funzionale e riduce l'accumulo di danni al DNA sia in modelli cellulari sia in modelli murini di SLA. Analogamente, in un modello di neurodegenerazione retinica in *Drosophila melanogaster*, la sovraespressione di Dicer-2, ma non di Dicer-1, attenua significativamente il fenotipo neurodegenerativo, suggerendo che i piccoli RNA prodotti da DICER esercitino un effetto neuroprotettivo attraverso un meccanismo dipendente dai siRNA.

Complessivamente, questi risultati indicano che il ripristino della DDR e della biogenesi dei DDRNA rappresenta una promettente strategia terapeutica per limitare la neurodegenerazione associata all'accumulo di inclusioni di TDP-43 e FUS nella SLA. [1] (Fig. 5)

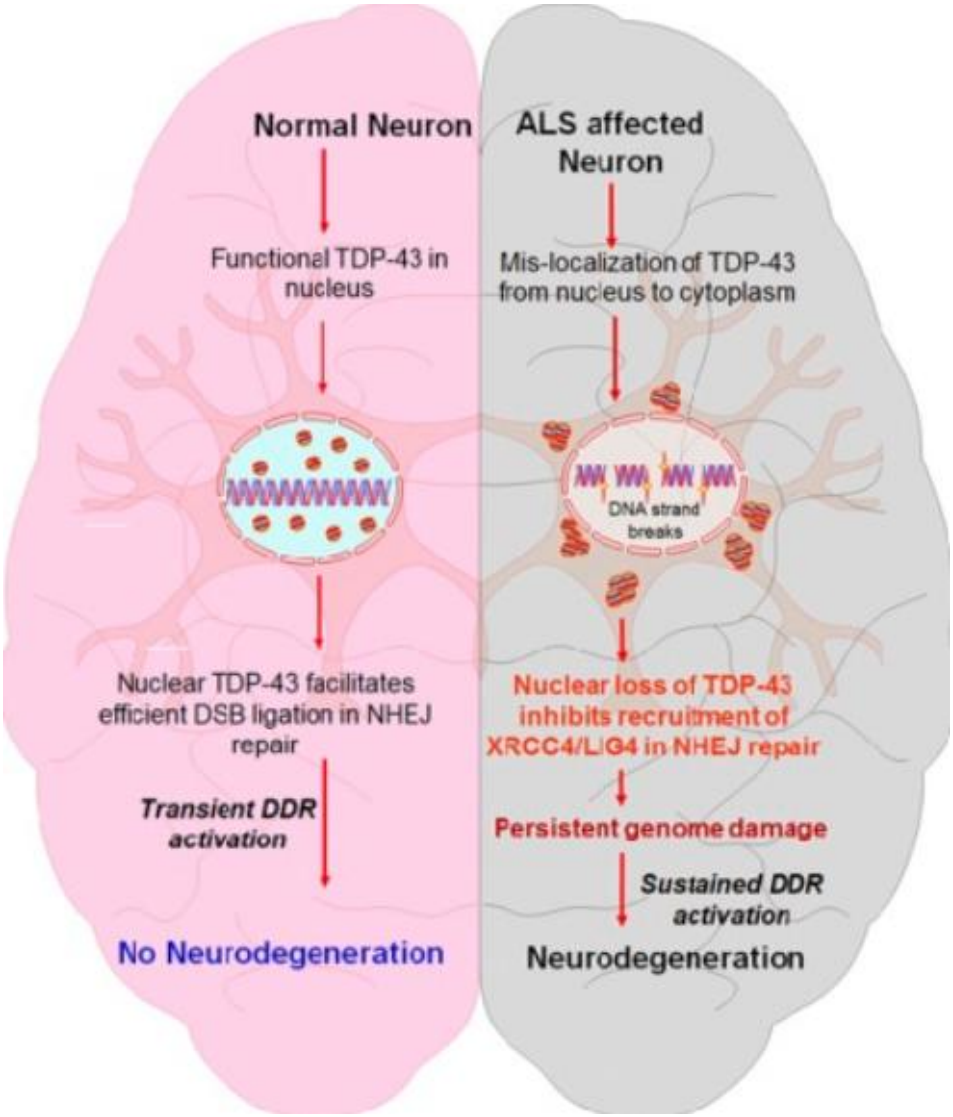

*Figura 6: Modello schematico che illustra il danno genomico seguito da un'attivazione persistente della risposta al danno del DNA (DDR) nei motoneuroni del midollo spinale affetti da **sclerosi laterale amiotrofica (SLA)**, causata dalla patologia di **TDP-43**. Nei neuroni sani, **TDP-43** rappresenta un componente essenziale della riparazione delle rotture a doppio filamento del DNA mediata dalla via **NHEJ**. La delocalizzazione nucleo-citoplasmatica di **TDP-43** nei motoneuroni compromette la riparazione delle DSB e contribuisce alla neurodegenerazione nella SLA. I risultati ottenuti evidenziano un collegamento tra la patologia di **TDP-43** e la compromissione della riparazione delle DSB, suggerendo potenziali strategie terapeutiche mirate ai meccanismi di riparazione del DNA per la **SLA associata a TDP-43**.*

Nonostante lo studio metta in evidenza 2 mutazioni genetiche particolarmente rilevanti nella malattia della SLA, è importante ricordare che solo il 10% dei casi

di SLA è familiare. Infatti, nella sALS gli individui affetti sono generalmente gli unici della famiglia con questa condizione, anche se in circa il 10-20% dei casi sono presenti più di un familiare con la stessa patologia, suggerendo fattori di rischio genetici.

Anche l'epigenetica quindi diventa un fattore essenziale da prendere in considerazione, in quanto esposizioni ambientali a sostanze tossiche e pesticidi, infezioni come l'HIV, particolari stili di vita e abitudini alimentari, il sesso maschile e il fumo possono favorire l'insorgenza della malattia o accelerarne il decorso.
Patologie complesse come la SLA sono il risultato di un'architettura poligenica, cioè varianti genetiche differenti sono associate alla patologia. Queste varianti possono essere integrate in un punteggio del rischio poligenico che, insieme alla valutazione ponderata di altri fattori come l'uso di medicinali, l'essere un fumatore, l'età e il peso, può accuratamente fornire una previsione sullo sviluppo della malattia e sulla reazione individuale dei diversi pazienti a una possibile terapia. [7]
Nello studio analizzato, però, non sono state prese in considerazione le variabili appena citate; non è possibile dedurre quindi l'influenza di tali variabili sull'effetto dell'enoxacina come strategia di recupero farmacologico.

BIBLIOGRAFIA

1. Modafferi S, Farina S, Esposito F, Brandi O, Di Salvio M, Della Valle I, D'Uva S, Scarian E, Cicio G, Riccardi A, Pisati F, Garbelli A, Santini T, Pansarasa O, Morlando M, D'Ambrosi N, Cozzolino M, Cestra G, d'Adda di Fagagna F, Gioia U, Francia S. DNA damage response defects induced by the formation of TDP-43 and mutant FUS cytoplasmic inclusions and their pharmacological rescue. Cell Death Differ. 2025 Dec;32(12):2309-2322. doi: 10.1038/s41418-025-01530-7. Epub 2025 May 29. PMID: 40437235; PMCID: PMC12669588.

2. Chen S, Sayana P, Zhang X, Le W. Genetics of amyotrophic lateral sclerosis: an update. Mol Neurodegener. 2013 Aug 13;8:28. doi: 10.1186/1750-1326-8-28. PMID: 23941283; PMCID: PMC3766231.

3. Cytion.com

4. Cabrini M, Roncador M, Galbiati A, Cipolla L, Maffia A, Iannelli F, Sabbioneda S, d'Adda di Fagagna F, Francia S. DROSHA is recruited to DNA damage sites by the MRN complex to promote non-homologous end joining. J Cell Sci. 2021 Mar 22;134(6):jcs249706. doi: 10.1242/jcs.249706. PMID: 33558311; PMCID: PMC8015226.

5. Mitra J, Guerrero EN, Hegde PM, Liachko NF, Wang H, Vasquez V, Gao J, Pandey A, Taylor JP, Kraemer BC, Wu P, Boldogh I, Garruto RM, Mitra S, Rao KS, Hegde ML. Motor neuron disease-associated loss of nuclear TDP-43 is linked to DNA double-strand break repair defects. Proc Natl Acad Sci U S A. 2019 Mar 5;116(10):4696-4705. doi: 10.1073/pnas.1818415116. Epub 2019 Feb 15. PMID: 30770445; PMCID: PMC6410842.

6. Lopes I, Altab G, Raina P, de Magalhães JP. Gene Size Matters: An Analysis of Gene Length in the Human Genome. Front Genet. 2021 Feb 11;12:559998. doi: 10.3389/fgene.2021.559998. PMID: 33643374; PMCID: PMC7905317.

7. Sharma R, Khan Z, Mehan S, Das Gupta G, Narula AS. Unraveling the multifaceted insights into amyotrophic lateral sclerosis: Genetic underpinnings, pathogenesis, and therapeutic horizons. Mutat Res Rev Mutat Res. 2024 Jul-Dec;794:108518. doi: 10.1016/j.mrrev.2024.108518. Epub 2024 Nov 2. PMID: 39491718.

8. Rothstein JD, Keeley O, Warlick C, Miller TM, Ly CV, Glass JD, Coyne AN. Sporadic ALS induced pluripotent stem cell derived neurons reveal hallmarks of TDP-43 loss of function. Nat Commun. 2025 Aug 2;16(1):7092. doi: 10.1038/s41467-025-62482-7. PMID: 40753166; PMCID: PMC12318032.

9. Michelini F, Pitchiaya S, Vitelli V, Sharma S, Gioia U, Pessina F, Cabrini M, Wang Y, Capozzo I, Iannelli F, Matti V, Francia S, Shivashankar GV, Walter NG, d'Adda di Fagagna F. Damage-induced lncRNAs control the DNA damage response through interaction with DDRNAs at individual double-strand breaks. Nat

Cell Biol. 2017 Dec;19(12):1400-1411. doi: 10.1038/ncb3643. Epub 2017 Nov 27. PMID: 29180822; PMCID: PMC5714282.
10. Chen Y, Yang M, Deng J, Chen X, Ye Y, Zhu L, Liu J, Ye H, Shen Y, Li Y, Rao EJ, Fushimi K, Zhou X, Bigio EH, Mesulam M, Xu Q, Wu JY. Expression of human FUS protein in Drosophila leads to progressive neurodegeneration. Protein Cell. 2011 Jun;2(6):477-86. doi: 10.1007/s13238-011-1065-7. Epub 2011 Jul 12. PMID: 21748598; PMCID: PMC3563268.

CDDpress

www.nature.com/cdd

ARTICLE OPEN

Check for updates

DNA damage response defects induced by the formation of TDP-43 and mutant FUS cytoplasmic inclusions and their pharmacological rescue

Stefania Modafferi[1,12], Stefania Farina[1,11,12], Francesca Esposito[1,12], Ornella Brandi[1,12], Michela Di Salvio[2], Ilaria Della Valle[3], Sara D'Uva[4], Eveljn Scarian[5], Giada Cicio[6], Adelaide Riccardi[1], Federica Pisati[7], Anna Garbelli[1], Tiziana Santini[4], Orietta Pansarasa[5], Mariangela Morlando[4], Nadia D'Ambrosi[8], Mauro Cozzolino[9], Gianluca Cestra[2,10], Fabrizio d'Adda di Fagagna[1,6], Ubaldo Gioia[1,6]✉ and Sofia Francia[1]✉

Formation of cytoplasmic inclusions (CIs) of TDP-43 and FUS, along with DNA damage accumulation, is a hallmark of affected motor neurons in Amyotrophic Lateral Sclerosis (ALS). However, the impact of CIs on DNA damage response (DDR) and repair in this pathology remains unprobed. Here, we show that CIs of TDP-43 and FUS^{P525L}, co-localizing with stress granules, lead to a dysfunctional DDR activation associated with physical DNA breakage. Inhibition of the activity of the DDR kinase ATM, but not of ATR, abolishes DDR signaling, indicating that DNA double-strand breaks (DSBs) are the primary source of DDR activation. In addition, cells with TDP-43 and FUS^{P525L} CIs exhibit reduced DNA damage-induced RNA synthesis at DSBs. We previously showed that the two endoribonucleases DROSHA and DICER, also known to interact with TDP-43 and FUS during small RNA processing, contribute to DDR signaling at DSBs. Treatment with enoxacin, which stimulates DDR and repair by boosting the enzymatic activity of DICER, restores a proficient DDR and reduces DNA damage accumulation in cultured cells with CIs and in vivo in a murine model of ALS. In *Drosophila melanogaster*, Dicer-2 overexpression rescues TDP-43-mediated retinal degeneration. In summary, our results indicate that the harmful effects caused by TDP-43 and FUS CIs include genotoxic stress and that the pharmacological stimulation of the DNA damage signaling and repair counteracts it.

Cell Death & Differentiation (2025) 32:2309–2322; https://doi.org/10.1038/s41418-025-01530-7

INTRODUCTION

Amyotrophic Lateral Sclerosis (ALS) is a neurodegenerative disease characterized by the progressive loss of the upper and lower motor neurons due to neuronal cell death [1]. Analogously to other neurodegenerative disorders like Frontotemporal Dementia (FTD) and Alzheimer's disease (AD), ALS is defined as a proteinopathy since motor neurons of patients affected by this pathology harbor aberrant protein aggregates in their cytoplasm [2]. 90% of ALS cases are sporadic (sALS), thus lacking a familial history, while the remaining ALS cases are characterized by autosomal dominant, autosomal recessive, or X-linked mutations occurring in specific genes, leading to familial inheritance (familial ALS, fALS) [3]. Notably, around 3% of fALS-associated mutations fall in the gene encoding for TAR DNA-binding protein 43 (TDP-43) and 6% in the gene for fused in sarcoma (FUS) and often follow an autosomal dominant inheritance pattern [3, 4]. Some mutations, particularly FUS^{P525L}, are believed to confer to these proteins an increased predisposition to form cytosolic aggregates [5]. Nevertheless, in the vast majority of both sALS and fALS and in FTD cases, TDP-43 accumulates in cytoplasmic inclusions (CIs) in its wild-type form [6]. In vivo, expression of mutant or wild-type human TDP-43 causes reduced locomotor activity and progressive paralysis in mice, and decreased lifespan in fruit flies [4]. FUS mutations also lead to a range of phenotypes affecting the nervous system, including defects in neuronal development, locomotion problems, reduced survival, and neurodegeneration in various model organisms [7]. FUS and TDP-43 knockout mice (FUS$^{-/-}$ and TARDBP$^{-/-}$, respectively) are often perinatal lethal while heterozygous animals exhibit motor symptoms [7, 8]. FUS$^{-/-}$ mice also show male sterility, defects in B-lymphocyte development, increased genomic instability and vulnerability to ionizing radiation [7].

TDP-43 and FUS are two RNA-binding proteins (RBPs) that cover multiple functions in RNA metabolism. They are both involved in

[1]Institute of Molecular Genetics "Luigi Luca Cavalli-Sforza", National Research Council (CNR), Pavia, Italy. [2]Institute of Molecular Biology and Pathology, CNR, Rome, Italy. [3]PhD Program in Cellular and Molecular Biology, Department of Biology, University of Rome Tor Vergata, Rome, Italy. [4]Department of Biology and Biotechnologies "Charles Darwin", Sapienza University of Rome, Rome, Italy. [5]Cellular Models and Neuroepigenetics Unit, IRCCS Mondino Foundation, Pavia, Italy. [6]IFOM ETS—The AIRC Institute of Molecular Oncology, Milan, Italy. [7]Cogentech Società Benefit srl, Milan, Italy. [8]Department of Biology, University of Rome Tor Vergata, Rome, Italy. [9]Institute of Translational Pharmacology, CNR, Rome, Italy. [10]Fondazione Policlinico Universitario A. Gemelli IRCCS, Università Cattolica del Sacro Cuore, Rome, Italy. [11]Present address: Department of Life, Health and Environmental Sciences, University of L'Aquila, L'Aquila, Italy. [12]These authors contributed equally: Stefania Modafferi, Stefania Farina, Francesca Esposito, Ornella Brandi. ✉email: ubaldo.gioia@cnr.it; sofia.francia@cnr.it

Received: 13 August 2024 Revised: 8 May 2025 Accepted: 19 May 2025
Published online: 29 May 2025

microRNA (miRNA) biogenesis, through their interaction with the endoribonuclease DROSHA [9, 10]. Moreover, FUS also exhibits a transcriptional regulatory role and can directly bind to the C-terminal domain (CTD) of RNA polymerase II (RNAPII) [11, 12]. Both TDP-43 and FUS are structurally characterized by the presence of low complexity domains (LCDs), which allow the two proteins to undergo liquid-liquid phase separation (LLPS), essential for the formation of insoluble membrane-less organelles, including stress granules (SGs) [13].

SGs are generated in response to different stress sources, with the proposed function of pausing protein synthesis until the stress ends [14]. Along with their constitutive components, like TIA-1 and G3BP1, SGs may include TDP-43 and FUS [14]. Interestingly, TDP-43 depletion alters both G3BP1 and TIA-1 levels and affects SG structure and dynamics [15]. Besides, motor neurons derived from induced pluripotent stem cells (iPSCs) carrying the FUS^{P525L} mutation display an increased number and altered kinetics of SG assembly [16].

Genome integrity ensures the maintenance of the genetic information against possible unfaithful transmission across generations. Both physiological events and environmental factors can cause DNA breaks [17]. Therefore, cells have developed a complex pathway named DNA Damage Response (DDR), which immediately detects the DNA lesion, signals its formation and ensures a proper DNA repair [18]. In particular, following double-strand break (DSB) formation, the multiprotein complex MRN (MRE11-RAD50-NBS1) binds the DNA ends, thus recruiting and activating ATM, a member of the phosphatidylinositol 3-kinase-related kinase (PIKK) family [19]. ATM, in turn, initiates the DDR signaling by phosphorylating the histone variant H2AX, which in its phosphorylated version is referred to as γH2AX [20]. Upon accumulation of single-strand breaks (SSBs), generally occurring during replication stress, H2AX is phosphorylated by ATR, another PIKK [21]. Initial γH2AX chromatin decoration creates a positive feedback loop that fuels further spreading of γH2AX and sequential accumulation of DDR proteins [20], including 53BP1, which plays a pivotal role in orchestrating the choice of DSB repair pathways [22].

Different neurodegenerative diseases, including ALS, have been associated with a high accumulation of DNA lesions in the nucleus of motorneurons [23, 24], affecting their viability. Intriguingly, a role for TDP-43 and FUS in DNA repair has been recently identified in loss of function model systems [25, 26]. For instance, the knockdown of either FUS or TDP-43 has been found to generate DNA breaks via RNAPII transcription stalling and the formation of DNA:RNA hybrids [27, 28]. Additionally, TDP-43 depletion hampers the recruitment to DSBs of the XRCC4-DNA ligase IV complex, which is crucial for the non-homologous end-joining (NHEJ) DNA repair pathway [25]. Similarly, FUS loss reduces the association of the repair protein Ku70 to DSB sites, and the recruitment of XRCC1/LIG3 to SSBs, resulting in the accumulation of unrepaired DNA lesions [25]. Instead, the impact of the formation of TDP-43- and FUS-containing SGs on genome integrity and DDR activation remains unknown.

In the present study, we investigate the molecular mechanisms underlying defects in DDR activation and the consequent accumulation of DNA damage following the formation of TDP-43 and FUS CIs. We also provide evidence that demonstrate that DDR components are potential therapeutic targets to mitigate the neurotoxic effects of TDP-43 and FUS proteinopathies.

RESULTS

Formation of TDP-43 and mutant FUS cytoplasmic inclusions (CIs) is associated with DNA damage accumulation

To acutely induce the formation of CIs in human cultured cells, we transiently transfected HeLa cells with plasmids expressing wild-type (WT) FUS and its ALS-linked mutant form (FUS^{P525L}), along with WT TDP-43 and two ALS-related mutant derivatives (TDP-43^{A382T} and TDP-43^{I383V}), in parallel with an empty vector (EV) as a control. Western blot analyses confirmed that the amounts of the ectopically expressed wild-type and mutant TDP-43 and FUS proteins were comparable to their endogenous levels (Fig. S1A, B). We next probed for FUS and TDP-43 subcellular localization by immunofluorescence (IF), using antibodies against the endogenous proteins. Although both FUS and TDP-43 were predominantly nucleoplasmic, they segregated into CIs (bright cytoplasmic puncta positive for FUS or TDP-43) in approximately 30% and 15–20% of the cells overexpressing FUS^{P525L} and TDP-43, respectively (Fig. S1C–F). Differently, the fraction of cells showing endogenous TDP-43-positive CIs was much lower (less than 3%) in samples transfected with the EV (Fig. S1C, E). Importantly, FUS segregated to CIs only upon the expression of its mutant version, while it was retained in the nucleus in WT FUS-expressing cells (Fig. S1D, F). Differently, ALS-linked mutations of TDP-43 did not further increase the tendency of this protein to form CIs (Fig. S1C, E). This observation aligns with the prevalence of WT TDP-43 inclusions in most ALS patients [6]. Consistently with previous reports [29], the expression of FUS^{P525L} and TDP-43 induced the formation of SGs, as determined by IF through the co-staining for the SG markers TIA-1 and G3BP1 (Fig. S1G). Importantly, the majority of FUS^{P525L} and TDP-43 CIs colocalized with such organelles (Fig. S1G, H), as also observed in ALS brain tissues [29]. Since the formation of CIs upon expression of either WT or mutant TDP-43 did not exhibit significant differences (Fig. S1C, E), and given our research focus on investigating the impact of CI formation on DDR activation and DNA repair, we exclusively conducted experiments using cells expressing WT TDP-43 for the rest of this study.

We then investigated the effects of CI formation on DNA damage accumulation at single-cell resolution by treating FUS- or TDP-43-expressing cells with Neocarzinostatin (NCS)—a radiomimetic drug largely used to acutely generate DSBs [30, 31]—followed by IF analysis. Notably, localization of FUS^{P525L} or TDP-43 into CIs was not affected by NCS administration (Fig. S1C–F), indicating that DNA damage is not the cause of FUS^{P525L} or TDP-43 aggregation, but rather a consequence. WT FUS- or EV-transfected cells presented little endogenous DNA damage and properly formed γH2AX-positive DDR foci upon treatment with NCS (Fig. 1A, B). Differently, a robust accumulation of pan-nuclear γH2AX signal was observed in cells with mutant FUS and TDP-43 CIs (Fig. 1A, B). Such a massive amount of γH2AX occurred even in the absence of exogenously inflicted DNA damage (Fig. 1A, B), indicating that the formation of CIs following FUS^{P525L} or TDP-43 expression was sufficient to induce a significant genotoxic stress. This intense γH2AX signal prevents from distinguishing discrete γH2AX foci in NCS-treated cells (Fig. 1A, B). Importantly, adjacent cells without mutant FUS- or TDP-43 CIs did not display pan-nuclear γH2AX signal, both in undamaged and damaged conditions (Fig. 1A, B). Augmented γH2AX levels are indicative of an increase of unrepaired DSBs. Thus, to specifically detect DSB accumulation following FUS or TDP-43 expression, we performed a neutral comet assay in cells not exposed to exogenous DNA damage and transfected with EV, FUS, FUS^{P525L} or TDP-43. Interestingly, we observed that the expression of TDP-43 or FUS^{P525L} increased the comet tail moment, suggestive of a higher amount of DSBs, compared to EV-transfected samples or cells overexpressing WT FUS (Fig. 1C, D).

These results indicate that the elevated γH2AX signal observed in the nucleus of cells with mutant FUS- or TDP-43- CIs is associated with a significant increase of physical DNA breakage in the form of DSBs.

ATM is hyper-activated and responsible for the increased γH2AX levels in cells with CIs

As soon as the DNA damage is sensed, the apical kinases ATM and ATR are engaged and trigger the local phosphorylation of H2AX,

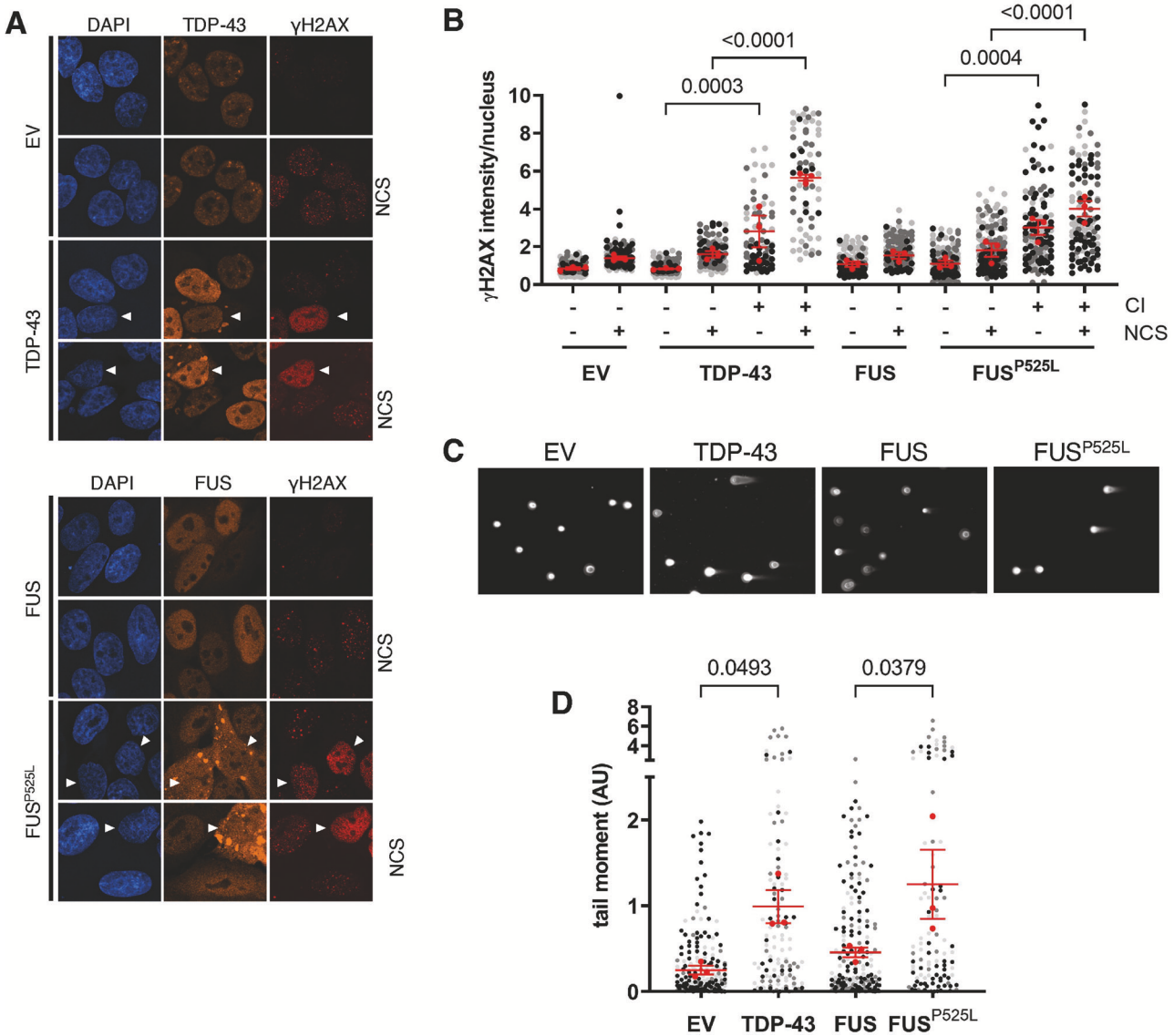

Fig. 1 Cells with TDP-43 or FUS^{P525L} cytoplasmic inclusions (CIs) show elevated γH2AX levels and increased DSB formation. A Analysis by immunofluorescence (IF) of γH2AX signals (red) in damaged (NCS) or undamaged HeLa cells transfected with plasmids expressing TDP-43, FUS or FUS^{P525L}. Cells transfected with an empty vector (EV) were used as a control. TDP-43 and FUS signals are shown in orange; nuclei were counter-stained with DAPI (blue). Arrowheads mark cells with CIs. **B** Super-plot showing the quantification of γH2AX intensity in HeLa cells with or without cytoplasmic inclusions (± CI) determined in (**A**). Red dots represent the mean values of each biological replicate; red bars indicate the averages ± SEM of three independent experiments. **C** Representative images of comet assay experiments performed in undamaged HeLa cells transfected as in (**A**). **D** Tail moment analysis of HeLa cells shown in (**C**). The red dots of the super-plot represent the mean values of each biological replicate; red bars indicate the averages ± SEM of three independent experiments.

along with several other protein targets [20, 21]. A previous study showed that pan-nuclear γH2AX accumulates in response to ATM activation in different contexts of chromatin structure alteration [32]. Instead, ATR activation has been occasionally associated with γH2AX pan-nuclear signal during replication stress [33, 34]. Thus, to determine which of these two kinases was responsible for γH2AX accumulation observed, we treated cells expressing FUS^{P525L}, TDP-43, or control samples, with specific ATM or ATR kinase activity inhibitors (KU60019 or VE-821, respectively [35]) and monitored their impact on γH2AX signals by IF. The specificity of inhibition of the two DDR kinases was confirmed by monitoring their auto-phosphorylation through immunoblotting (Fig. S2A). Intriguingly, ATM inhibition almost completely abrogated γH2AX signal in cells with TDP-43 or FUS^{P525L} CIs, compared to control samples treated with the vehicle (DMSO) (Fig. 2A, B). On the other hand, ATR inactivation had no effect in decreasing γH2AX levels in cells with FUS^{P525L}, while it marginally reduced γH2AX signal in those with TDP-43 CIs (Fig. 2A, B).

We also observed that cells not treated with NCS and harboring TDP-43 or FUS^{P525L} CIs exhibited an aberrantly diffused pATM signal, in contrast to those expressing TDP-43 or FUS^{P525L} but lacking CIs (Fig. 2C, D). This suggests that the formation of such aggregates is sufficient to trigger a diffused and aberrant ATM activation even without exogenous induction of DNA damage. In line with this, we also observed that ATM activation is inefficient in cells with CIs. While cells without FUS^{P525L} or TDP-43 CIs properly mounted pATM foci formation upon DSB induction following NCS treatment, cells harboring CIs showed a significantly lower number of pATM foci (Fig. 2C, E). When we next probed by IF for the activation by phosphorylation of the transducer kinase CHK2, an ATM substrate [36], CI-bearing cells displayed reduced pCHK2 signals upon NCS treatment (Fig. S2B, C).

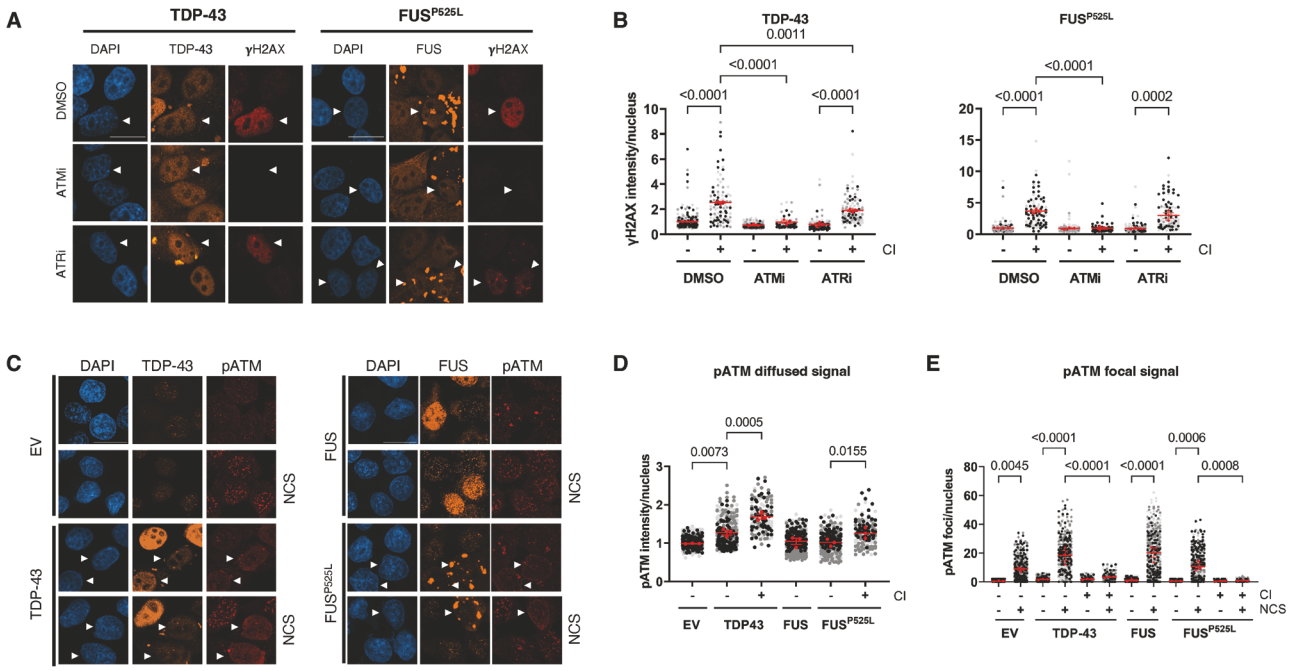

Fig. 2 ATM is aberrantly activated, and its inhibition abolishes pan-nuclear γH2AX formation in cells with TDP-43 and FUS^{P525L} CIs. **A** Analysis by immunofluorescence (IF) of γH2AX levels (red) in HeLa cells expressing TDP-43 or FUS^{P525L} and treated with ATMi or ATRi. Cells treated with DMSO were used as a control. TDP-43 and FUS are labeled in orange; nuclei were counter-stained with DAPI. Arrowheads mark cells with CIs; scale bar = 10 µm. **B** Quantification of γH2AX intensity in HeLa cells with or without cytoplasmic inclusions (±CI) described in (**A**). The red dots of the super-plots represent the mean values of each biological replicate; red bars indicate the averages ± SEM of three independent experiments. **C** IF analysis of pATM signal (red) in HeLa cells transfected with plasmids expressing an empty vector (EV), TDP-43 or FUS^{P525L}. TDP-43 and FUS are labeled in orange; nuclei were counter-stained with DAPI. Arrowheads mark cells with CIs; scale bar = 10 µm. **D**, **E** Quantification of diffused and focal pATM signal (**D**, **E**, respectively) in HeLa cells with or without cytoplasmic inclusions (± CI) determined in (**C**). The red dots of the super-plot represent the mean values of each biological replicate; red bars indicate the averages ± SEM of three independent experiments.

In sum, these results indicate that the accumulation of pan-nuclear γH2AX detected in CI-bearing cells relies on a dysfunctional ATM activation, which is responsible for pan-nuclear γH2AX levels but does not efficiently transmit the DDR signal to downstream effector kinases, such as CHK2.

Previous evidence indicates that pan-nuclear γH2AX marks cells in S-phase upon UV-irradiation [37] and correlates with DNA replication defects [34]. Intriguingly, TDP-43 was shown to associate with replication forks in normal conditions, protecting cells from replicative stress [38]. Although we observed that ATR, involved in regulating DDR during DNA replication, was dispensable for γH2AX accumulation (Fig. 2A, B), we tested if the γH2AX signal observed in cells with FUS^{P525L} or TDP-43 CIs might be elicited by replicative stress. To this end, we initially examined the capacity of CI-bearing cells to de novo synthesize DNA, by performing a 5-bromo-2′-deoxyuridine (BrdU) incorporation assay followed by IF. We observed that cells with FUS^{P525L} or TDP-43 CIs incorporated much less BrdU, compared to those without CIs or with samples expressing WT FUS or the EV (Fig. S2D, E). Similarly, we observed that all the cells harboring FUS^{P525L}- or TDP-43-positive CIs had very low or null levels of Cyclin A (Fig. S2F), which is expressed in the S/G2-phase of the cell cycle [39, 40], suggesting that such cells were preferentially in G1-phase and not replicating. To confirm this, we took advantage of Fluorescent, Ubiquitination-based Cell Cycle Indicator (FUCCI)-expressing HeLa cells [41], which allow cell cycle phases to be readily visualized by fluorescent microscopy. These cells were transfected with plasmids expressing either TDP-43, FUS or FUS^{P525L}, or with an empty vector (EV) as a control. We observed that the vast majority of cells presenting TDP-43 and FUS^{P525L} CIs (96 and 91%, respectively) were G1-positive (i.e., expressing the G1 marker CDT1, labeled in orange; Fig. S2G, H). In contrast, only 60–70% of cells without CIs or those expressing wild-type FUS or EV were G1-positive (Fig. S2G, H). These results, which are in line with those obtained through BrdU and Cyclin A staining, further support the impact of CI formation on impeding G1-S transition.

In summary, we found that CI formation causes DNA damage accumulation and an aberrant ATM activation, which in turn prevent cells from initiating DNA synthesis and entering the S-phase of the cell cycle.

FUS^{P525L} and TDP-43 CIs hamper the phosphorylation and the recruitment of 53BP1 to DSBs

53BP1 is one of the main mediators of the DDR cascade and it is involved in DNA repair by NHEJ, which is the pathway used by non-replicating cells, including neurons, to repair DSBs [42]. Since we previously observed that DDR initiation, as detected by probing for the auto-phosphorylation of ATM, was altered in cells with both FUS^{P525L} and TDP-43 CIs (Fig. 2C–E), we tested if the recruitment of 53BP1 was also defective in such cells. While NCS-treated cells without CIs mounted 53BP1 foci, cells with FUS^{P525L} or TDP-43 CIs were unable to form 53BP1 foci upon NCS treatment (Fig. 3A, B).

Following DSB formation, 53BP1 is phosphorylated by ATM at multiple S/T-Q motifs to modulate DDR and repair [43, 44]. We therefore monitored by IF 53BP1 phosphorylation in NCS-treated FUS^{P525L}- or TDP-43-expressing cells. We observed that CI-containing cells showed significantly less p53BP1 foci compared to those without aggregates (Fig. 3C, D). Differently from what we observed for pATM (Fig. 2C, D), undamaged CI-bearing cells showed low or no p53BP1 signal (Fig. 3C, D). Also, TDP-43 and FUS^{P525L} aggregation did not substantially affect 53BP1 total levels (Fig. S3A), indicating that CIs negatively impacted on 53BP1

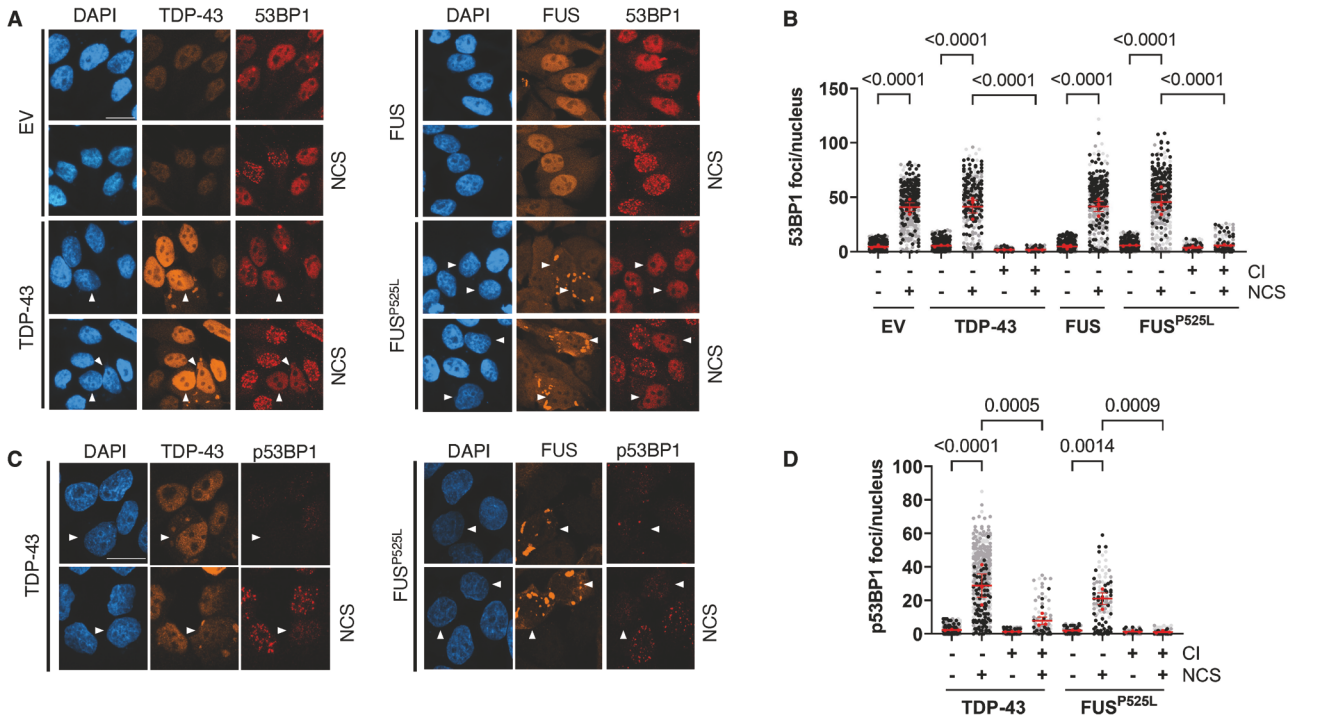

Fig. 3 DDR signaling and 53BP1 activation is impaired in cells with TDP-43 and FUS^{P525L} CIs. A, **C** Representative images of 53BP1 and p53BP1 (red) in damaged (NCS) or undamaged HeLa cells transfected with plasmids encoding for TDP-43, FUS or FUS^{P525L}. Cells transfected with an empty vector (EV) were used as a control. TDP-43 and FUS are shown in orange; nuclei were counter-stained with DAPI. Arrowheads mark cells with CIs; scale bar = 20 µm. **B**, **D** Quantification of DDR marker signals in cells with or without cytoplasmic inclusions (± CI) determined in (**A**, **C**), respectively. The red dots of the super-plots shown in (**B**, **D**) represent the mean values of each biological replicate; red bars indicate the averages ± SEM of three independent experiments.

activation, rather than on its expression. Overall, these results suggest that the hyper-activation of ATM caused by CI formation is unable to transduce the signal to the downstream DDR mediator 53BP1.

The scaffold protein MDC1 plays a key role in the DSB signaling, ensuring the recruitment of the E3-ubiquitin ligases RNF8 and RNF168, which in turn allows the assembly of 53BP1 at DSBs [45]. Specifically, MDC1 associates to the site of damage mostly in a γH2AX-dependent manner [46] and, differently from 53BP1, functions upstream to both homologous recombination (HR), a repair pathway exploited by replicating cells, and NHEJ [47]. To probe for the impact of CI formation on the ability of MDC1 to localize at DSBs, we stained TDP-43- and FUS^{P525L}-expressing cells and their controls for MDC1. Differently from 53BP1, NCS-treated cells with TDP-43 or FUS^{P525L} CIs showed normal damage-induced MDC1 foci formation (Fig. S3B, C).

Taken together, these results indicate that the two DDR mediator proteins, 53BP1 and MDC1, behave differently in cells bearing mutant FUS or TDP-43 CIs, with the profound defect in 53BP1 foci formation not being accompanied by reduced MDC1 focal recruitment.

Since the expression of TDP-43 and FUS^{P525L} triggered the assembly of SGs (Fig. S1G, H), we tested if their formation was sufficient to alter DDR and cause DNA damage accumulation. To this end, we acutely treated HeLa cells with sodium arsenite ($NaAsO_2$), an inorganic compound commonly used to promote SG assembly [48]. After incubating the samples with 500 µM $NaAsO_2$ for 30 min, nearly all cells exhibited cytoplasmic SGs, as detected by IF against the SG marker TIA-1 (Fig. S3D). Notably, when we examined DNA damage accumulation and DDR activation in these samples, we observed that undamaged (–NCS) $NaAsO_2$-treated cells did not show pan-nuclear γH2AX signals (Fig. S3D, E). Moreover, damaged (i.e., with NCS) and $NaAsO_2$-treated cells were able to mount a proper response to DSB formation, with 53BP1 foci levels comparable to those of untreated (i.e., without $NaAsO_2$) cells (Fig. S3D, E). In summary, these results suggest that SG assembly alone is not sufficient to compromise genome integrity or DDR activation, unlike the formation of cytoplasmic inclusions of TDP-43 or FUS^{P525L}.

Transcription is repressed in cells with TDP-43 or FUS^{P525L} CIs

TDP-43 and FUS functions have been linked to transcription modulation [28]. Moreover, ongoing transcription is halted in response to DSBs, to allow proper DNA damage resolution and preserve genome integrity [49–52]. Specifically, ATM has been shown to initiate transcriptional repression in response to DSB formation [49]. We thus wondered if the increased levels of DNA damage observed in cells with TDP-43 and FUS CIs also correlated with transcriptional inhibition. To monitor de novo transcription in cells with CIs, we labeled nascent RNAs in TDP-43- and FUS^{P525L}-expressing cell cultures with 5-Ethynyl-Uridine (EU) using a "click-chemistry" approach followed by fluorescent microscopy analysis. We observed a significantly lower EU incorporation signal in cells with either TDP-43 or FUS^{P525L} CIs, indicating a global transcriptional repression (Fig. 4A, B).

Since our results indicate that ATM inactivation was sufficient to inhibit γH2AX accumulation in CI-containing cells (Fig. 2A, B), we tested its potential impact on global transcription in cells with CIs. We therefore pharmacologically inhibited the ATM kinase activity in HeLa cells expressing TDP-43 or FUS^{P525L} and monitored nascent RNA synthesis using the assay described above. We observed that ATM inhibition elevated the EU signal in cells with CIs, compared to those treated with the vehicle only (Fig. S4A, B). These results therefore indicate that the accumulation of CIs causes an ATM-dependent repression of global transcription.

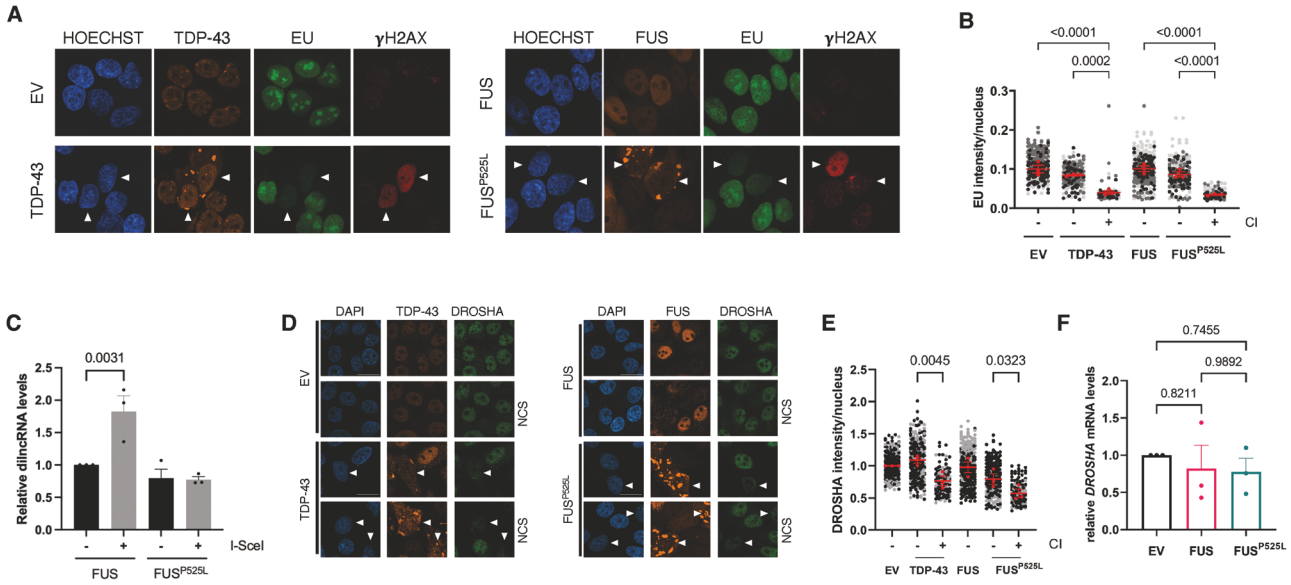

Fig. 4 Transcription is halted in cells with TDP-43 and FUS^{P525L} CIs. A HeLa cells expressing TDP-43, FUS or FUS^{P525L} were pulse-labeled with EU and analyzed by immunofluorescence; TDP-43 and FUS, EU and γH2AX are shown in orange, green and red, respectively. Nuclear DNA was visualized using Hoechst dye; arrowheads mark cells with CIs. **B** Quantification of EU signal in cells with or without cytoplasmic inclusions (± CI) shown in (**A**). The red dots of the super-plot represent the mean values of each biological replicate; red bars indicate the averages ± SEM of three independent experiments. **C** Damage-induced long non-coding RNA (dilncRNA) expression was studied by strand-specific RT-qPCR in cut (I-SceI +) or uncut (I-SceI -) I-HeLa111 cells selected for the presence of FUS or FUS^{P525L} CIs through FACS. The histogram shows dilncRNA levels normalized over RPLP0 mRNA and shown as relative to the uncut FUS-expressing sample; values are the means ± SEM of three independent experiments. **D** Representative images of DROSHA expression (green) in damaged (NCS) or undamaged HeLa cells transfected with plasmids encoding for TDP-43, FUS or FUS^{P525L}; cells transfected with an empty vector (EV) were used as a control. TDP-43 and FUS are labeled in orange; nuclei were counter-stained with DAPI. Arrowheads mark cells with CIs; scale bar = 10 µm. **E** Quantification of DROSHA protein levels in cells with or without cytoplasmic inclusions (± CI) from panel (**D**). The red dots of the super-plot represent the mean values of each biological replicate; red bars indicate the averages ± SEM of three independent experiments. **F** *DROSHA* mRNA levels were monitored by RT-qPCR in HeLa cells selected for the presence of FUS or FUS^{P525L} CIs through FACS. Values are the averages ± SEM of three independent experiments.

Biogenesis of damage-induced non-coding RNAs is defective in CI-containing cells

Following DSB formation, while pre-existing transcription is repressed, RNAPII is recruited at sites of DNA damage where it drives the local synthesis of damage-induced long non-coding RNAs (dilncRNAs) [35, 53]. Such transcripts can be further processed by DROSHA and DICER to generate DNA damage response RNAs (DDRNAs) that, along with dilncRNAs, control DDR activation and DNA repair [35, 53–55]. We thus investigated if the transcriptional repression observed in CI-containing cells (Fig. 4A, B) also impacted on dilncRNA biogenesis. To accomplish this, we profiled the expression of dilncRNAs in I-HeLa111 cells, where a traceable DSB can be generated at a genomic I-SceI recognition site by expressing the I-SceI meganuclease [56]. To enrich and selectively study dilncRNA levels in cells bearing CIs, we took advantage of the Bimolecular Fluorescence Complementation (BiFC) approach [57]. Specifically, we transfected I-HeLa111 cells with two constructs expressing FUS^{P525L} fused to two distinct fragments of the GFP fluorescent protein, mVenus and mCerulean, that emit a fluorescent signal only when brought into proximity with each other upon FUS protein dimer formation, and even more when FUS aggregates [57] (Fig. S4C). Highly fluorescent cells were in this way enriched by fluorescence-activated cell sorting (FACS) and total RNA was isolated from sorted cells and analyzed for dilncRNA expression by strand-specific RT-qPCR. Upon DSB induction with I-SceI, I-HeLa111 cells expressing WT FUS showed elevated dilncRNA levels, while those expressing FUS^{P525L} failed to induce dilncRNAs following DSB generation (Fig. 4C).

As mentioned above, along with DICER, the endoribonuclease DROSHA participates in DDRNA biogenesis, and associates with DSBs where it is required for 53BP1 recruitment and repair by NHEJ [54, 58–60]. We noticed that cells containing TDP-43 and FUS^{P525L} CIs displayed reduced DROSHA protein levels, compared to those devoid of aggregates (Fig. 4D, E). To determine whether CI formation impacted on *DROSHA* expression at the RNA level, we measured the amounts of *DROSHA* mRNA by RT-qPCR in cells with FUS aggregates using the BiFC system. We observed no change in its levels in samples expressing FUS^{P525L} compared to control cells (Fig. 4F), suggesting that FUS aggregation rather affected DROSHA protein stability. Contrarily, DICER protein levels were not significantly altered in cells with inclusions (Fig. S4D, E).

Taken together, these results indicate that the formation of cytoplasmic aggregates is accompanied by a defective biogenesis of damage-induced non-coding RNAs, important modulators of DDR activation.

TDP-43 and FUS cytoplasmic aggregation correlates with defective DDR, DNA damage accumulation and reduced DROSHA levels in neuronal lines

The findings we have presented so far were generated using the HeLa cervical carcinoma cell line. However, TDP-43 and FUS dysfunction are particularly toxic to neurons. Therefore, we examined if the formation of TDP-43 and FUS CIs impacted DDR activation and DNA damage accumulation in neuronal lines as well. To this end, we first employed SH-SY5Y human neuroblastoma cells, which are routinely used as a cellular model to study the molecular mechanisms underlying the development of neurodegenerative diseases [27, 61, 62]. We thus transfected SH-SY5Y cells with plasmids expressing wild-type TDP-43, FUS, or FUS^{P525L}, or with an empty vector as a control. The cells were then treated with or without NCS, and DDR activation was monitored in cells containing or lacking CIs. Unfortunately, FUS^{P525L}-transfected SH-SY5Y cells displayed very few inclusions (not shown), which prevented us from generating

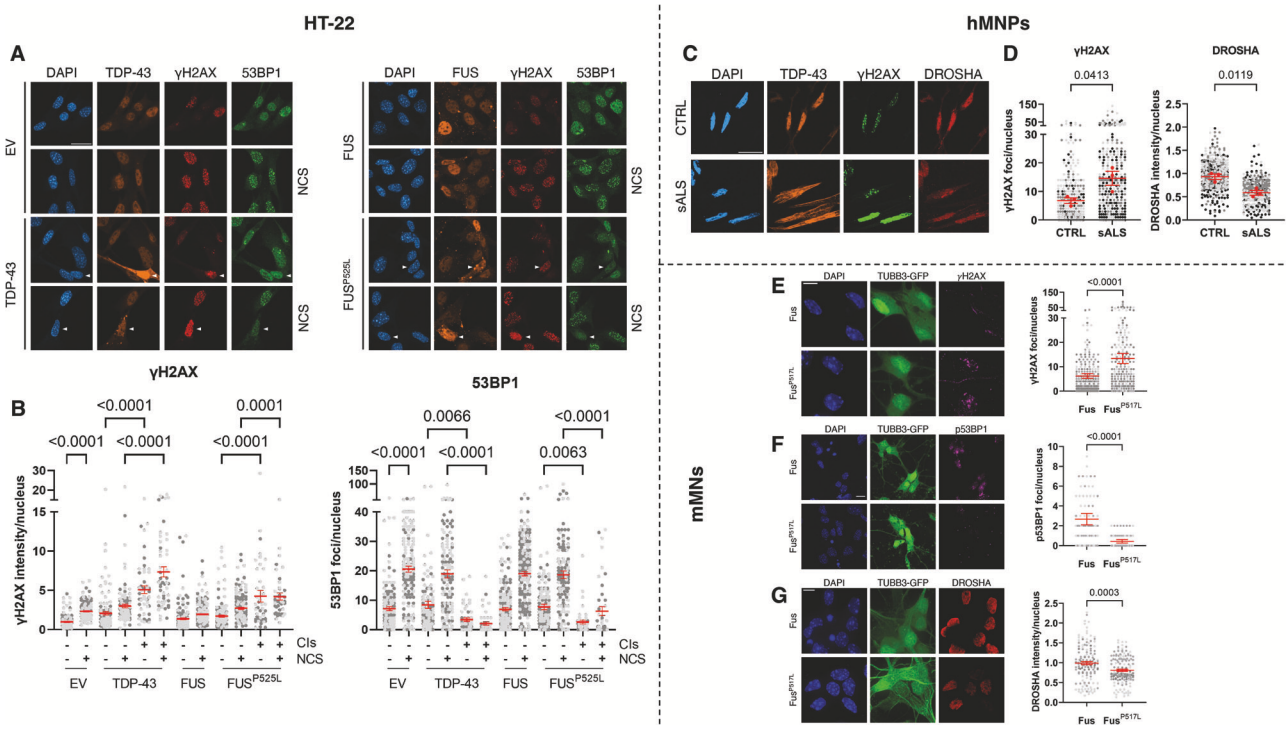

Fig. 5 TDP-43 and FUS cytoplasmic aggregation correlates with an altered DDR, DNA damage accumulation and reduced DROSHA levels in neuronal cell lines. A Analysis by immunofluorescence (IF) of γH2AX (red) and 53BP1 (green) signals in damaged (NCS) or undamaged HT-22 cells expressing TDP-43, FUS or FUS^{P525L}; cells transfected with the empty vector (EV) were also examined. TDP-43 and FUS are shown in orange; nuclei were counter-stained with DAPI (blue); arrowheads mark cells with CIs. Scale bar = 20 µm. **B** Dot-plot showing γH2AX intensity (left) and 53BP1 foci (right) in HT-22 cells with or without cytoplasmic inclusions (± CIs), as determined in (**A**); red bars indicate the averages ± SEM; at least 40 cells were scored for each condition in two independent experiments. **C** Analysis by IF of γH2AX (green) and DROSHA (red) signals in hMNPs derived from sALS or a healthy (CTRL) donor; endogenous TDP-43 (orange) is also shown. Nuclei are counter-stained with DAPI (blue); scale bar = 20 µm. **D** Quantification of γH2AX foci (left) and DROSHA levels (right) in hMNPs, as determined in (**C**). The red dots of the super-plot represent the mean values of each biological replicate; red bars indicate the averages ± SEM of three independent experiments. **E** TUBB3-GFP-expressing mMNs carrying wild-type or mutant Fus were stained for γH2AX. The dot-plot shows γH2AX foci in each nucleus; red bars indicate the averages ± SEM; at least 150 cells were scored for each condition in three independent experiments. **F** IF analysis of p53BP1 foci in mMNs. The dot-plot shows p53BP1 foci in each nucleus; red bars indicate the averages ± SEM. At least 60 cells were scored for each condition in two independent experiments. **G** IF analysis of DROSHA protein levels in mMNs. The dot-plot shows DROSHA intensity in each nucleus; red bars indicate the averages ± SEM. At least 130 cells were scored for each condition in three independent experiments. **E–G** nuclei were counter-stained with DAPI; scale bar = 100 µm.

informative and robust results. On the bright side, and as observed in HeLa cells, transfection with the plasmid expressing TDP-43 led to the formation of CIs co-localizing with SGs in SH-SY5Y cells, albeit at a much lower frequency compared to HeLa cells (Fig. S5A, D). Similarly, SH-SY5Y cells containing TDP-43 CIs displayed increased γH2AX levels (Fig. S5B, C). In addition, SH-SY5Y cells bearing TDP-43 CIs and treated with NCS showed reduced 53BP1 foci compared to cells without CIs (Fig. S5B, C). These results confirm that the formation of TDP-43 CIs impairs 53BP1 recruitment and causes DNA damage accumulation also in this neuronal tumor cell line. Additionally, as already shown in HeLa cells (Fig. S2F), TDP-43 CI-containing SH-SY5Y cells displayed reduced Cyclin A expression, suggesting that TDP-43 CI formation impacted on cell cycle progression in these cells as well (Fig. S5D, E). Next, we extended these studies to HT-22 mouse hippocampal neuronal cells. Consistent with the results obtained in HeLa and in SH-SY5Y cell lines, HT-22 cells harboring TDP-43 and FUS^{P525L} CIs exhibited increased γH2AX signals, compared to those lacking CIs (Fig. 5A, B). Moreover, in CI-containing HT-22 cells, 53BP1 focus formation following NCS administration was severely impaired (Fig. 5A, B). In this non-tumoral neuronal line, we also tested if CI formation triggered p53 activation by probing for its phosphorylated form (p-p53^{S15}) through IF. We noticed that CI-containing HT-22 cells did not exhibit augmented p-p53^{S15} signals, compared to cells without CIs (Fig. S5F, G). This indicates that CI formation did not cause p53 activation.

Then, we sought to validate our results in other relevant neuronal lines, namely human motor neuron progenitors (hMNPs) and mature murine motor neurons (mMNs). hMNPs were generated from induced pluripotent stem cells (iPSCs) of a sALS patient or a healthy donor (Fig. S5H) [63]. sALS hMNPs, characterized by a marked TDP-43 cytoplasmic delocalization, showed augmented γH2AX signals and reduced DROSHA levels, compared to control hMNPs (Fig. 5C, D). mMNs carrying on both alleles the FUS^{P517L} mutation, which is equivalent to human FUS^{P525L}, present a strong FUS signal in the cytoplasm, whereas FUS is almost exclusively localized to the nucleus of wild-type mMNs (Fig. S5I) [64]. Notably, FUS^{P517L}-expressing mMNs exhibited increased γH2AX, reduced p53BP1 foci, and diminished DROSHA signals with respect to control mMNs (Fig. 5E–G).

In summary, these results confirm that alterations of TDP-43 and FUS subcellular distribution are associated to dysfunctional DDR, accumulation of DNA damage and decreased DROSHA levels in neuronal cells as well.

Enoxacin restores proficient DDR, reduces DNA damage accumulation, and partially restores transcription in CI-bearing cells

Enoxacin is a small molecule able to enhance the enzymatic activity of the endoribonuclease DICER, involved in the processing of different classes of short RNAs, including small interfering RNAs (siRNAs) and

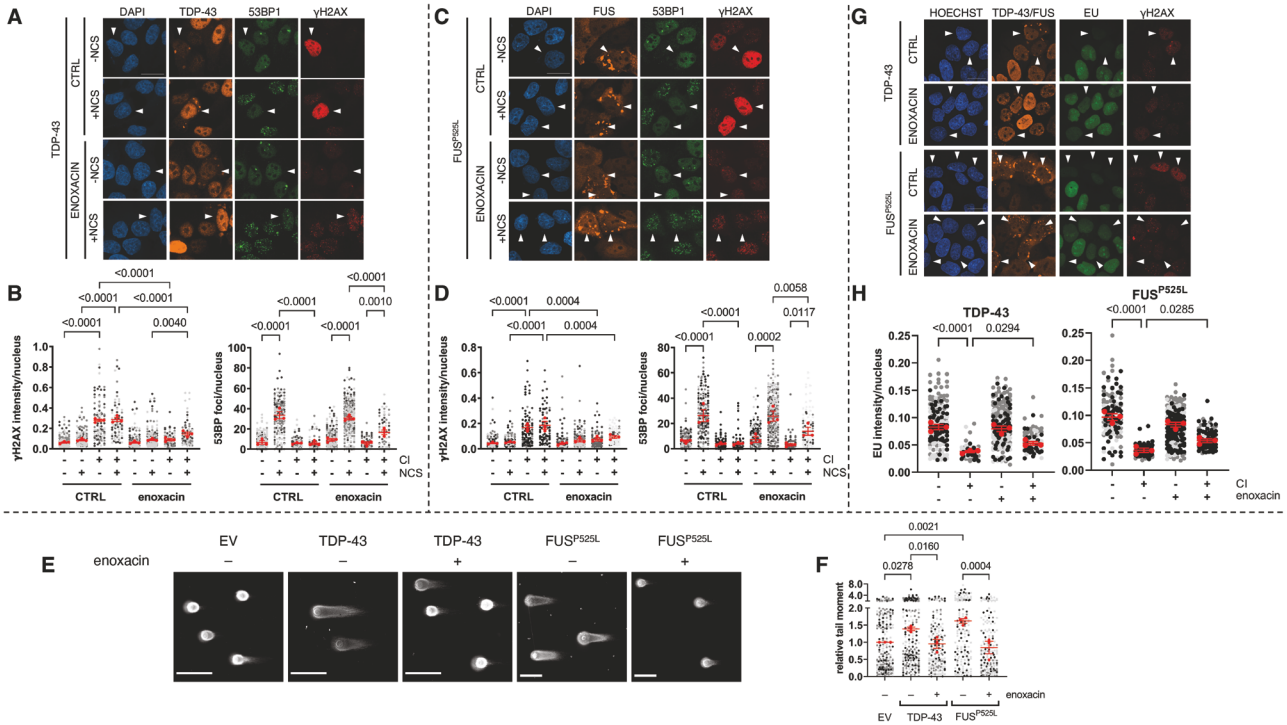

Fig. 6 Enoxacin rescues foci formation and partially restores transcription in cells with TDP-43 and FUS^{P525L} CIs. A, **C** HeLa cells expressing TDP-43 or FUS^{P525L} were treated or not with enoxacin prior to NCS administration and analyzed by immunofluorescence for DDR activation; TDP-43 and FUS are labeled in orange. Nuclei were counter-stained with DAPI; arrowheads mark cells with CIs. Scale bar = 10 µm. **B**, **D** Quantification of γH2AX intensity and 53BP1 foci in cells with or without cytoplasmic inclusions (±CI) shown in (**A**, **C**), respectively. The red dots of the super-plots represent the mean values of each biological replicate; red bars indicate the averages ± SEM of three independent experiments. **E** Representative images of comet assay experiments performed in undamaged HeLa cells transfected with the plasmid expressing TDP-43, FUS^{P525L}, or an empty vector (EV) and treated or not with enoxacin; scale bar = 100 µm. **F** Tail moment analysis of HeLa cells shown in E. The red dots of the super-plot represent the mean values of each biological replicate; red bars indicate the averages ± SEM of three independent experiments. **G** HeLa cells expressing TDP-43 or FUS^{P525L} were treated or not with enoxacin and pulse-labeled with EU prior to immunofluorescence analysis; TDP-43 and FUS are shown in orange. Nuclear DNA was visualized using Hoechst dye; arrowheads mark cells with CIs. Scale bar = 10 µm. **H** Quantification of EU signal in cells with or without cytoplasmic inclusions (±CI) determined in (**G**). The red dots of the super-plot represent the mean values of each biological replicate; red bars indicate the averages ± SEM of three independent experiments.

miRNAs [65, 66]. In this regard, enoxacin treatment has been shown to promote the biogenesis of DICER-dependent small RNAs [65, 66] and we previously demonstrated it stimulates DDR signaling and DNA repair in cultured cells [55, 61, 67, 68]. Therefore, we tested if enoxacin administration could restore proper DDR activation and reduce DNA damage accumulation in cells with CIs. HeLa cells were treated with enoxacin for 48 h prior to transfection with TDP-43 or FUS^{P525L} expressing plasmids and monitored for 53BP1 and γH2AX signals by IF. Enoxacin-treated cells bearing TDP-43 and FUS^{P525L} CIs showed both increased 53BP1 foci and reduced γH2AX levels, compared to untreated samples (Fig. 6A–D). In addition, supplementing enoxacin to cells expressing TDP-43 or FUS^{P525L} decreased DSBs back to normal levels, as revealed by comet assay (Fig. 6E, F). These results therefore demonstrate that enoxacin can restore DDR function and reduce DNA damage accumulation in cells with CIs.

Since transcription was inhibited in CI-containing cells (Fig. 4A, B), we tested whether enoxacin administration could also restore proficient transcription in these cells. Thus, we performed the EU incorporation assay described above in enoxacin-treated cells expressing either TDP-43 or FUS^{P525L} and we observed that enoxacin treatment significantly increased the levels of EU incorporation in cells harboring CIs, in comparison to untreated CI-bearing cells, although not to the level detected in cells devoid of CIs (Fig. 6G, H).

Altogether, these results show that enoxacin improves DDR and DNA repair in cells with TDP-43 or FUS^{P525L} aggregates, leading to restored global transcription.

Enoxacin stimulates DDR and lowers DNA damage accumulation in an ALS murine model of FUS pathology

We then sought to extend and validate the observations obtained in cultured cells in in vivo models of ALS pathology. To this aim, we administrated enoxacin to either non-pathological heterozygous or pathological homozygous mice over-expressing the wild-type human homolog of FUS (hFUS) [69, 70] and probed for DDR activation and damage accumulation, by staining murine spinal cords for γH2AX and 53BP1 by immunohistochemistry (IHC) technique. Consistent with our results in cultured cells, hFUS homozygous mice presented higher levels of γH2AX and reduced 53BP1 signals in their spinal cord, with respect to heterozygous animals (Fig. 7A, B). Importantly, in enoxacin-treated homozygous mice we observed that the signal of 53BP1 increased, whereas γH2AX levels decreased, compared to vehicle-treated animals (Fig. 7A, B).

Taken together, these exciting results suggest that enoxacin administration in vivo in mice with FUS pathology was effective in stimulating DDR, reducing DNA damage accumulation.

DICER overexpression counteracts neurodegeneration in a *Drosophila melanogaster* ALS model system

Our results in mice show that the enhancement of DNA repair through enoxacin administration reduces DNA damage accumulation in vivo. However, how this can impact on neurodegeneration remains unexplored. To test this, we used a *Drosophila melanogaster* model of TDP-43-mediated neurotoxicity, in which the ectopic

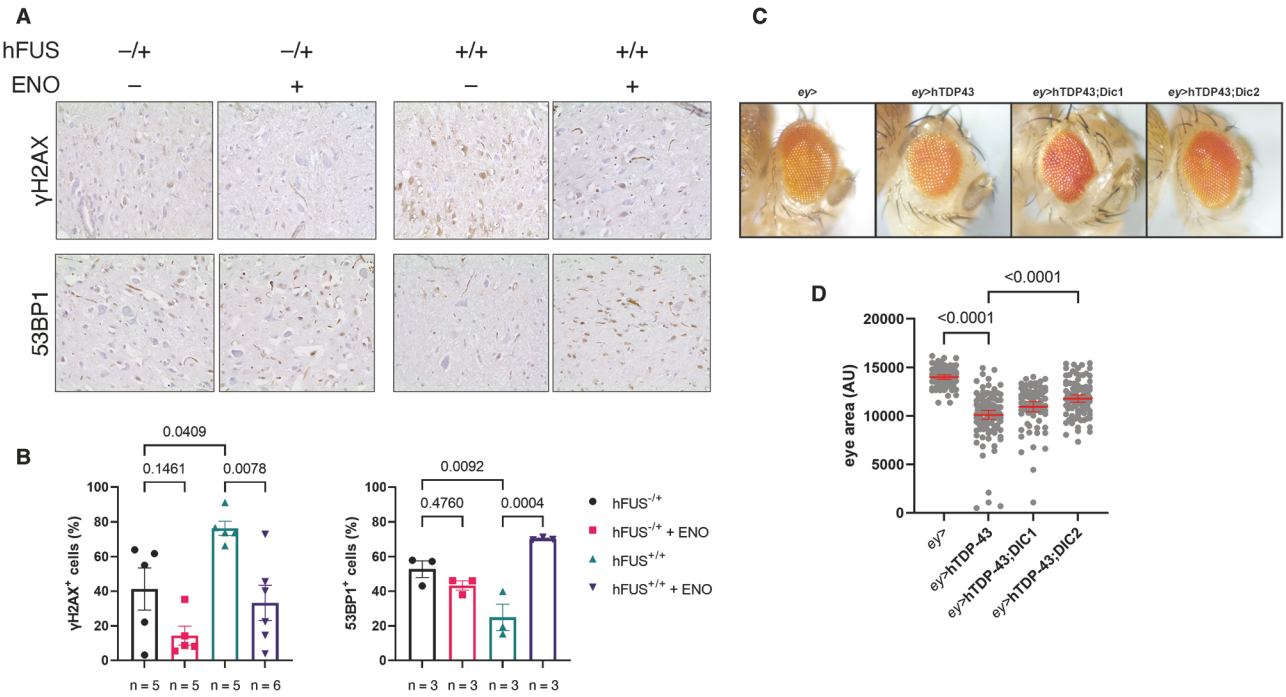

Fig. 7 Enoxacin stimulates DDR and reduces DNA damage accumulation in hFUS murine spinal cords. Dicer-2 overexpression counteracts retina degeneration in hTDP-43 *Drosophila melanogaster* eyes. A Representative IHC images of spinal cords of hFUS-expressing mice, treated with enoxacin or vehicle and stained for γH2AX and 53BP1. **B** Quantification of the percentage of cells positive for the indicated markers as determined in (**A**). Values are the means ± SEM. At least three mice were studied for each condition; the precise number is indicated below each histogram. **C** Representative images of *Drosophila melanogaster* eyes from adult flies expressing the indicated constructs under control of eyeless-GAL4. **D** Dot plot showing the quantification of mean eye area of the flies with the indicated genotypes; more than 70 eyes per genotype were analyzed in three independent experiments; red bars represent the means ± SEM.

expression of the human TDP-43 (hTDP-43) in the fly ommatidia causes progressive retinal degeneration, as shown by a significant reduction of the eye area, which is not associated to a diminished proliferation of ommatidial cells in the larvae [71] (Figs. 7C, D, S6). To mimic the effects of enoxacin administration in this system, we overexpressed both *D. melanogaster* isoforms of Dicer in hTDP-43-expressing flies and monitored their impact on retinal degeneration. Differently from mammals, the *D. melanogaster* genome encodes for two distinct Dicer enzymes: Dicer-1, mainly involved in cytoplasmic miRNA biogenesis, and Dicer-2 with a more prominent role in siRNA processing in the nucleus [72]. Remarkably, the overexpression of Dicer-2 significantly rescued the eye area in hTDP-43-expressing flies (Fig. 7C, D). Conversely, no major effects were observed in flies co-expressing hTDP-43 and Dicer-1, ruling out a central role for miRNAs in preventing retinal degeneration (Fig. 7C, D).

These results indicate that stimulating Dicer functions may be beneficial in counteracting TDP-43-mediated neurodegeneration.

DISCUSSION

Accumulation of unrepaired DNA damage and the resulting disruption of genome integrity can have profound consequences, including ageing and inflammation, which in turn increase the susceptibility to various pathological conditions, especially neurodegenerative diseases [25, 73, 74]. In light of this, mounting evidence have recently put into relation DNA damage repair defects with neurodegeneration in ALS [25]. ALS is characterized by an aberrant accumulation of insoluble cytoplasmic inclusions (CIs) containing TDP-43 and other RNA-binding proteins, including FUS [2]. Interestingly, endogenous wild-type FUS and TDP-43 have been reported to play crucial roles in DNA damage repair [75]: FUS associates with DNA lesions by interacting with PAR-chains generated at damaged chromatin [76], and favors DNA damage resolution by recruiting the XRCC1/LIG3 repair complex to DNA lesions [77]. In addition, recently, TDP-43 has been implicated in DNA repair and reported to associate at DSBs with factors of the NHEJ machinery, ultimately contributing to DNA damage resolution in physiological conditions [62]. These studies have highlighted a causative link between the depletion of FUS and TDP-43 with genome instability and reduced survival in neuronal cells [62, 77]. Nonetheless, the impact of TDP-43 and FUS cytoplasmic aggregation—a pathological hallmark of ALS—on DNA damage accumulation has not been fully elucidated.

Here, we show that the deposition of TDP-43 and FUS^{P525L} CIs, which are associated with stress granules (SGs) (Fig. S1G, H), triggers a dysfunctional DDR (Figs. 2C–E, 3 and 5A, B), and induces DSB accumulation (Fig. 1). Differently, cells overexpressing FUS or TDP-43, but devoid of CIs, do not accumulate DNA damage (Figs. 1A, B and 5A, B) and display proficient DDR when exogenous DNA damage is inflicted (Figs. 2C–E, 3 and 5A, B). Specifically, cells accumulating CIs display a hyper-activation of the apical DDR kinase ATM, responsible for the massive increase of the pan-nuclear γH2AX signal observed (Fig. 2). Such aberrant activation of ATM is however unable to transduce the signal to the downstream DDR and repair factors, including 53BP1 (Fig. 3), ultimately hampering their recruitment to DNA damage sites and consequently preventing DNA damage resolution through NHEJ, the predominant DNA repair pathway in non-dividing cells. Importantly, ATM inhibition using small molecules prevents the accumulation of DNA damage signals in cells with CIs (Fig. 2A, B). Interestingly, ATR inactivation had a little but significant impact in reducing γH2AX levels in cells with TDP-43 CIs, but not in those containing FUS^{P525L} inclusions (Fig. 2A, B). Such discrepancy can be explained by the fact that dysfunctional TDP-43 has been associated with DNA replication defects, possibly leading to ATR activation [38]. Consequently, ATR may contribute, at least partly, to the augmented γH2AX signal observed in cells containing TDP-

43 CIs. We also noticed that the induction of SG formation by acute treatment with $NaAsO_2$ was not sufficient to cause a DDR defect or DNA damage accumulation (Fig. S3D, E). This observation is consistent with the finding that acute administration of $NaAsO_2$ to ALS fibroblasts leads to the formation of SGs lacking TDP-43, whereas a prolonged $NaAsO_2$ exposure induces the assembly of SGs containing TDP-43 inclusions [78]. Our results therefore indicate a causative relationship between TDP-43 and FUS inclusions in SGs and genotoxicity.

Shutdown of global transcription is one of the immediate consequences of DNA damage generation [79]. In particular, the activation by auto-phosphorylation of ATM in response to DNA damage has been shown to enforce chromatin modifications surrounding DSBs, which in turn prevent RNAPII elongation [49]. Loss of either TDP-43 and FUS has been linked to transcription arrest and consequent formation of DNA damage at sites of active transcription [28]. Consistent with this, cells harboring TDP-43 or FUS^{P525L} CIs display dysfunctional ATM hyperactivation (Fig. 2C–E) and pan-nuclear γH2AX signals (e.g., Figs. 1A, B, 2A, B and 4A) and exhibit reduced global transcription (Fig. 4A, B). Pharmacological inactivation of ATM rescues proficient RNA synthesis in CI-containing cells (Fig. S4A, B). Overall, our results indicate that TDP-43 or FUS^{P525L} CI formation, by inducing aberrant DDR and DSB generation, hampers transcription. In this regard, we noticed that CI formation does not engage p53 activation, as determined by probing for its ATM/ATR-dependent phosphorylation at serine 15 (p-p53) through immunofluorescence in HT-22 cells (Fig. S5F, G). Moreover, TDP-43 and FUS aggregation caused cell cycle arrest and transcriptional inhibition also in HeLa cells, which express very low levels of p53 [80]. Our data therefore suggest that the events observed following CI formation occur in a p53-independent manner. Notably, CI-induced transcriptional repression may have profound implications particularly in neurons, where longer transcripts are enriched with respect to other cell types [81, 82]. In this regard, the inactivation of genes involved in regulating RNAPII processivity, by favoring the accumulation of truncated transcripts, has been associated to synaptic dysfunction, autism, and neurodegeneration [82]. Such findings, along with the results shown here, provide an intriguing explanation for the higher sensitivity of neural tissues to CI accumulation, compared to others.

Interestingly, the formation of cytosolic aggregates not only hampers the synthesis of damage-induced non-coding RNAs (Fig. 4C), but it might also impair their processing into DNA damage response RNAs (DDRNAs) by reducing the nuclear levels of DROSHA (Fig. 4D, E). Such events may ultimately interfere with faithful DNA damage resolution [35, 53, 60, 83], likely establishing a detrimental feedback loop that further exacerbates the accumulation of unrepaired DNA lesions. Accordingly, in this double-hit process, even minimal improvements in DDRNA biogenesis may exert beneficial effects.

The small molecule enoxacin, which was reported to enhance DICER activity [66], is one of the few compounds able to boost DDR and improve repair [55, 61, 67, 68]. Its administration was demonstrated effective in improving DNA damage resolution in irradiated primary mouse cortical neurons [55] and in an AD model of human neuronal cells [61]. In the present study, we show that stimulating DICER activity through enoxacin restored functional DDR and decreased DNA damage accumulation in HeLa cells with TDP-43 and FUS^{P525L} CIs, and in vivo in hFUS-expressing mice (Figs. 6A–F and 7A, B). To evaluate whether the observed effects of DICER enhancement on stimulating DDR and repair were also beneficial at counteracting neurotoxicity, we expressed both Dicer-1 and Dicer-2 in a *Drosophila melanogaster* model of TDP-43-mediated retinal neurodegeneration. Intriguingly, while the overexpression of Dicer-2 almost completely restored the normal fly eye size, Dicer-1 ectopic expression had no impact (Fig. 7C, D). This suggests that the small RNAs generated by DICER exert their function in controlling DDR and repair, ultimately promoting neuronal cell survival through an siRNA-mediated mechanism, rather than in a miRNA-like fashion.

In conclusion, our results strongly suggest that the factors involved in DDR may represent relevant pharmacological targets for the treatment of the cytotoxic effects caused by TDP-43 and FUS CIs.

MATERIALS AND METHODS

Cell culture and treatments

Cell lines were authenticated by STR profiling (GenePrint system, Promega) and tested for mycoplasma contamination. HeLa, FUCCI-HeLa and HT-22 cells were cultured in DMEM supplemented with 10% FBS, 1% L-glutamine and 1% penicillin/streptomycin (P/S). SH-SY5Y were cultured in DMEM/F12 supplemented with 15% FBS and 1% P/S. DNA damage was induced by treating cells with 50 ng/mL neocarzinostatin (NCS) (Sigma, #N9162) for 20 min at 37 °C. Stress granule formation was induced by treating HeLa cells with 500 µM of sodium arsenite ($NaAsO_2$) for 30 min at 37 °C. I-HeLa111 were cultured in DMEM supplemented with 10% tetracycline-free FBS, 1% L-glutamine and 1% P/S and selected regularly with G418 (1 mg/ml) and hygromycin B (300 µg/ml). In I-HeLa111, I-SceI-mediated double-strand breaks were generated by doxycycline administration (1 µg/ml) for at least 16 h. To inhibit ATM and ATR, cells were treated with 5 µM KU60019 and 10 µM VE-821 overnight, respectively. Where indicated, HeLa cells were treated with 50 µM enoxacin (Millipore, #557305-250MG) for 24 h prior to plasmid transfection and left until the end of the experiment (48 h in total).

Transfections

In total, 1–2 µg of each plasmid was transfected for 24 h using Lipofectamine 2000 (Invitrogen; #11668-027) according to the manufacturer instructions. The following plasmids were employed: pcDNA3.1+ (ThermoFisher) was used as an empty vector negative control; MYC-tagged WT TDP-43 expressing vector, a kind gift of Dr. Emanuele Buratti on concession of Dr. Leonard Petrucelli (Mayo Clinic, Jacksonville, Florida); FLAG-tagged WT FUS and FUS^{P525L} expressing plasmids. For the Bimolecular Fluorescence Complementation (BiFC) experiments, WT FUS or FUS^{P525L} were cloned in pCS2plus-mCerulean 156-239-GGGS (Addgene, #162616) and pCS2plus-mVenus1-155-GGGS (Addgene, #162610), both gift from Marco Morsch [57], using the Gibson Assembly kit (ThermoFisher). 0.7 µg of each vector were transfected using Lipofectamine 2000.

Immunofluorescence and image analysis

Immunofluorescence (IF) for DDR markers was performed as already described [54]. IF for TDP-43 and FUS was conducted with antibodies against the endogenous proteins (Supplementary Table 1), unless otherwise specified. Images were acquired using a confocal linear laser-scanning microscope (Zeiss LSM 800). Quantitative immunofluorescence analyses were performed in parallel with identical acquisition parameters and exposure times among conditions, using CellProfiler software [84]. To distinguish between cells with or without CIs, a unique number was assigned to each cell nucleus in every image with CellProfiler. DICER cytoplasmic signal was quantified using Fiji software (NIH). For a complete list of the antibodies used in this study see Supplementary Table 1.

Colocalization of TDP-43 and FUS with TIA-1 or G3BP1 was determined using JACoP plugin (http://rsb.info.nih.gov/ij/plugins/track/jacop.html) of Fiji software [85]. We calculated Manders' overlap coefficient (MOC), which represents the fraction of TDP-43 or FUS signals overlapping with TIA-1 or G3BP1 signals. The best-fit lower threshold was determined using the threshold tool and visually inspected. We considered the MOC of at least two biological replicates and performed at least 15 acquisitions per sample per replicate.

Immunoblotting

Immunoblotting analyses were conducted as shown previously [60]. Protein amounts were quantified using Image Lab 6.1 software (Bio-Rad). For a complete list of the antibodies used in this study see Supplementary Table 1. The full length uncropped original western blots used in this work are provided in the 'Supplemental Material' file.

Comet assay
To detect DSB formation in cultured cells, we performed a neutral comet assay as previously described [55].

BrdU incorporation assay
After plasmid transfection, cells were treated with 10 μM BrdU (MedChemExpress, #HY-15910/CS-2028) overnight and incubated at 37 °C. The following day, cells were washed twice in 1X PBS and fixed in 4% paraformaldehyde for 10 min at RT. Coverslips were then washed twice in 1X PBS and blocked in 1X PBG (0.5% bovine serum albumin, 0.2% gelatin from cold water fish skin (Sigma Aldrich, #G7765) in 1x PBS) for 1 h at RT. Next, coverslips were incubated for one hour at RT in a humid chamber with a 1X PBG mix containing an anti-BrdU primary antibody (BD Laboratories, #347580) diluted 1:20 and RQ1 DNAse (Promega, #M610A) and RQ1 DNAse buffer (Promega, #M198A), each diluted 1:10. After incubation of the primary antibody, cells were washed three times in 1X PBS and immunofluorescence continued as described above.

EU incorporation
5-EU incorporation experiments were performed as already described [86]. Briefly, following DNA damage generation via NCS treatment, nascent RNAs were labeled with 1 h pulse of 1 mM 5-EU. Cells were then fixed in 4% paraformaldehyde (PFA; ChemCruz; #sc-281692) and levels of EU incorporation were detected by Click-iT RNA imaging kit (Invitrogen; #C10330) according to the manufacturer's instructions.

Cell sorting
24 h post plasmid transfection, cells were washed twice with 1X PBS, gently scraped and collected in 1 mL of sorting buffer (2 mM EDTA, 20 mM HEPES pH 7.3 in 1X PBS) per condition, collected in 15 mL tubes and placed on ice. Next, samples were transferred onto a 5 mL falcon equipped with a 35 μM nylon mesh (Corning, #3532235) and vortexed thoroughly to dissociate any cell clusters that might have formed. Next, samples were analysed on an S3e Cell sorter (BioRad). 30000 cells transfected with the EV were analysed first to set the gates. Next, cells expressing WT or FUS^{P525L} were sorted in purity mode and the positive cells were collected. Following cell sorting, cells were centrifuged at 4 °C for 1.5 min at full speed and the supernatant was discarded. Cells were then either lysed to collect RNA or frozen at −80 °C for future use.

RT-qPCR
Total RNA extraction was performed using the miRNeasy Mini Kit (Qiagen, #1038703), according to the manufacturer's instructions. 1 μg of total RNA was reverse transcribed using the SuperScript IV First-Strand Synthesis System (Invitrogen, #18091050). For dilncRNA detection in I-HeLa111 cells, 500 ng of total RNA were reverse transcribed with the SuperScript III First-Strand Synthesis System (Invitrogen, #18080-51) using gene-specific primers. Then, samples were chilled on ice and incubated for 20 min at 37 °C with 1 μL of RNase H (Invitrogen). Real-time quantitative PCR (qPCR) reactions were performed on a LightCycler® 480 II Sequence Detection System (Roche) using QuantiTect SYBR® Green PCR kit (Qiagen; #204145). For a complete list of primers used in this study see Supplementary Table 2.

Human motor neuron progenitors (hMNPs)
Human neural stem cells (hNSCs) obtained from sex- and age-matched control and sporadic ALS iPSCs were differentiated into hMNPs as previously reported [63]. Briefly, hNSCs cultured in adhesion conditions were differentiated into hMNPs in 7 days using a medium composed of 2× Neurobasal (ThermoFisher Scientific, USA), 2× Advanced DMEM/F12, 50× Neural Induction Supplement (ThermoFisher Scientific, USA), 0,1 μM Retinoic Acid (RA) (Sigma-Aldrich, USA) and 0,5 μM Purmorphamine (ThermoFisher Scientific, USA).

Generation and analysis by immunofluorescence of mouse motor neurons (mMNs)
mMNs carrying wild-type or mutant FUS on both alleles were differentiated from mouse embryonic stem cells as described before [64]. Cells cultured for 2 days after embryoid body dissociation were replated on HCl 1 M, pre-washed and pre-coated glass coverslips (0.01% poly-L-ornithine, 20 mg/mL laminin) and fixed in 4% PFA (Electron Microscopy Sciences) /4% sucrose/ 5 mM MgCl2/1 X PBS for 30 min at 4 °C. Cells were then washed once in 2% sucrose/1 X PBS and then twice in 4% sucrose/1 X PBS. Following the dehydration steps with the room temperature ethanol (50%, 70%), cells were stored at +4 °C in absolute ethanol + 1:100 VRC (Sigma-Aldrich) until use or processed immediately. Cells were permeabilized 0.2% (0.25% for p53BP1 IF) Triton X-100 for 20 min at room temperature, blocked in 1% goat/1% donkey serum (2% BSA for p53BP1 IF)/PBS for 1 h and then incubated with anti-γH2AX (1:1000, Ab11174, Abcam), anti-phospho-53BP1 (1:500, 3364, Cell signaling), anti-DROSHA (1:500, 3364, Cell Signaling) or rabbit polyclonal anti-TLS/FUS (1:300, ab84078, Abcam) and anti-beta III tubulin (1:200, AB9354, Sigma-Aldrich) primary antibodies overnight at 4 °C. Subsequently, they were incubated with donkey anti-rabbit Alexa Fluor Plus 647 (A32795; Thermo Fisher Scientific) and goat anti-chicken Alexa 488 (SAB4600031, Sigma-Aldrich) secondary antibodies diluted 1:200 in 1% goat/1% donkey serum (2% BSA for p53BP1 IF)/PBS for 45 min at room temperature. After washing twice in 1X PBS, cells were incubated with DAPI solution for 5 min at room temperature and then mounted using ProLong Diamond Antifade Mountant. mMNs samples were imaged using an inverted confocal Olympus IX73 microscope equipped with a Crestoptics X-LIGHT V3 spinning disk system and a Prime BSI Express Scientific CMOS camera and with an Olympus iX83 FluoView1200 laser scanning confocal microscope. The acquisitions were obtained using a UPLANSApo 60X (NA 1.35) oil objective and a UPlanSApo 100× (NA 1.40) oil objective and were collected with the MetaMorph software (Molecular Devices). The z stack confocal microscopy images were taken automatically (200 nm Z-spacing) and merged with the maximum intensity projection method.

Mice
Mice were housed at the Tor Vergata University Animal Facility (CIMETA) in accordance with the FELASA Recommendations, European Guidelines for the use of animals in research (2010/63/EU), and Italian Laws (D.L. 26/2014). They were kept at constant temperature of 22 ± 1 °C, relative humidity of 50%, and a 12-h light cycle (7 a.m.–7 p.m.), with free access to food and water. To ensure nutrition and hydration, wet food was provided to cages where mice displayed signs of paralysis. Hemizygous Tg (Prnp-FUS) WT3Cshw/J mice expressing human wild-type FUS (hFUS ±, Jackson Laboratories), displaying no pathological signs, were backcrossed to obtain homozygous mice (hFUS+/+), models of ALS. Genotyping was performed as previously described [69]. All experiments were conducted in compliance with the ARRIVE guidelines, with the approval by the local ethics committee and the Italian Ministry of Health. Every effort was made to minimize mice suffering and reduce the number of mice used to obtain reliable results. A total of $n = 12$ hFUS mice (sex-mixed groups) were included in the study. They were treated intraperitoneally daily with either enoxacin at a dose of 10 mg/kg or with vehicle. Enoxacin (Millipore, #557305-250MG) was initially dissolved in 1 M NaOH solution to a concentration of 312 mM and then diluted 100× in PBS for injection. Vehicle was 10 mM NaOH in PBS. Treatment was initiated at about 26 days, which correspond to early symptoms onset in hFUS +/+ mice, for the following 8 days, until mice reached an advanced symptomatic stage (about 34 days). Mice were euthanized with CO_2, spinal cords were removed and fixed in a 4% paraformaldehyde (PFA) for 12 h and finally immersed in a 30% sucrose solution in PBS.

Immunohistochemistry
Immunohistochemistry staining was conducted as shown before [87]. For each section studied, five non-overlapping fields were analyzed using the segmentation-based algorithm Multiplex IHC v3.2.3 of HALO software (Indica Labs).

Fly strains
Drosophila stocks and crosses were maintained on *Drosophila* standard medium (Nutri-fly, Genesee Scientific) at 25 °C. UAS-hTDP-43 fly line was gifted from Fabian Feiguin. Bloomington stock center (http://flybase.bio.indiana.edu/) provided the GAL4 driver and the other strains utilized: eyeless-GAL4 inserted on the second chromosome (5534 (w[*]; P{w[+m*]=GAL4-ey.H}3-8); both Dicer transgenes were inserted on the third chromosome (59022 (w*;P{UAS-Dcr-2.D}2,P{UAS-mCherry.CAAX.S}2;TM2/TM6B,Tb1)), and (36510 (y1w*;P{UAS-Dcr-1.D}3).

Analysis of Drosophila melanogaster eyes
Pictures of fly eyes were taken with the stereomicroscope (ZEISS Semi 508, 50X) equipped with Axiocam camera 105 and exploiting ZEISS ZEN

software (blue edition). Eye area was measured with the open-source software NIH ImageJ FIJI.

Drosophila eye disc labeling

Third instar eye discs were prepared, stained, and mounted following previously described protocols [88]. Briefly, larval brains were isolated by grabbing the mouth hooks with one pair of forceps while gently pulling the rest of the body with another pair of forceps, in a drop of physiological saline buffer. The eye and antennal imaginal discs remained attached to the brain via the hooks, which were used to transfer the samples into the fixation medium. Larval tissues were fixed for 1 h in fixation buffer (4% paraformaldehyde, 4% sucrose in phosphate buffer), permeabilized with permeabilization buffer (0,25% Triton-X in 1× PBS), and blocked in blocking solution (0,1% Triton-X, 3% BSA in 1× PBS). The following antibodies were used: anti-phospho-Histone H3 (Ser10) (Merck), diluted 1:500 was incubated overnight; donkey anti-rabbit Oregon Green (Jackson Immunoresearch), diluted 1:300. Immunofluorescence analysis was performed using an Axiophot epifluorescence microscope (Carl Zeiss), and fluorescence images were processed with Adobe Photoshop.

Statistical analysis

We did not use any criteria to determine the sample size. As much data as possible was collected depending on the nature of the experiments or in order to have statistical analysis. For animal studies, no statistical methods were used to estimate the sample size. For each experiment, we performed at least three biological replicates, unless stated otherwise; this information is reported in the figure legends.

For in vitro experiments, wells were randomly assigned into each group, and all cells were analyzed equally; for in vivo experiments in mice, animals were randomized to the experimental groups. No blinding method was applied, as we used unbiased software for data collection and analysis.

Prism 9 software (GraphPad) was used to generate graphs, perform statistical analysis and occasionally remove values with the Robust regression and Outlier removal method. Statistical analysis was performed using ordinary One-way ANOVA test, assuming equal SDs between the analyzed groups; unpaired two-tailed *t*-test was applied in Figs. 5D–G and S6B. The exact p-values, center values, and errors are indicated in each figure and its legends.

DATA AVAILABILITY

Source data are provided with this paper and available online. All other data that support the findings of this study are available from the corresponding authors on reasonable request.

REFERENCES

1. Taylor JP, Brown RH, Cleveland DW. Decoding ALS: from genes to mechanism. Nature. 2016;539:197–206.
2. Farina S, Esposito F, Battistoni M, Biamonti G, Francia S. Post-translational modifications modulate proteinopathies of TDP-43, FUS and hnRNP-A/B in amyotrophic lateral sclerosis. Front Mol Biosci. 2021;8:585.
3. Chen S, Sayana P, Zhang X, Le W. Genetics of amyotrophic lateral sclerosis: an update. Mol Neurodegener. 2013;8:1–15.
4. Lagier-Tourenne C, Polymenidou M, Cleveland DW. TDP-43 and FUS/TLS: emerging roles in RNA processing and neurodegeneration. Hum Mol Genet. 2010;19:46–64.
5. Conte A, Lattante S, Zollino M, Marangi G, Luigetti M, Del Grande A, et al. P525L FUS mutation is consistently associated with a severe form of juvenile Amyotrophic Lateral Sclerosis. Neuromuscul Disord. 2012;22:73–5.
6. Saberi S, Stauffer JE, Schulte DJ, Ravits J. Neuropathology of amyotrophic lateral sclerosis and its variants. Neurol Clin. 2015;33:855–76.
7. Shang Y, Huang EJ. Mechanisms of FUS mutations in familial amyotrophic lateral sclerosis. Brain Res. 2016;1647:65–78.
8. Kraemer BC, Schuck T, Wheeler JM, Robinson LC, Trojanowski JQ, Lee VMY, et al. Loss of Murine TDP-43 disrupts motor function and plays an essential role in embryogenesis. Acta Neuropathol. 2010;119:409–19.
9. Kawahara Y, Mieda-Sato A. TDP-43 promotes microRNA biogenesis as a component of the Drosha and Dicer complexes. Proc Natl Acad Sci USA. 2012;109:3347–52.
10. Morlando M, Dini Modigliani S, Torrelli G, Rosa A, Di Carlo V, Caffarelli E, et al. FUS stimulates microRNA biogenesis by facilitating co-transcriptional Drosha recruitment. EMBO J. 2012;31:4502–10.
11. Schwartz JC, Ebmeier CC, Podell ER, Heimiller J, Taatjes DJ, Cech TR. FUS binds the CTD of RNA polymerase II and regulates its phosphorylation at Ser2. Genes Dev. 2012;26:2690–5.
12. Tan AY, Manley JL. The TET family of proteins: functions and roles in disease. J Mol Cell Biol. 2009;1:82–92.
13. Li Z, Liu X, Liu M. Stress granule homeostasis, aberrant phase transition, and amyotrophic lateral sclerosis. ACS Chem Neurosci. 2022;13:2356–70.
14. Protter DSW, Parker R. Principles and properties of stress granules. Trends Cell Biol. 2016;26:668–79.
15. McDonald KK, Aulas A, Destroismaisons L, Pickles S, Beleac E, Camu W, et al. TAR DNA-binding protein 43 (TDP-43) regulates stress granule dynamics via differential regulation of G3BP and TIA-1. Hum Mol Genet. 2011;20:1400–10.
16. Lenzi J, De Santis R, De Turris V, Morlando M, Laneve P, Calvo A, et al. ALS mutant FUS proteins are recruited into stress granules in induced pluripotent stem cell-derived motoneurons. DMM Dis Models Mech. 2015;8:755–66.
17. Ciccia A, Elledge SJ. The DNA damage response: making it safe to play with knives. Mol Cell. 2010;40:179–204.
18. Jackson SP, Bartek J. The DNA-damage response in human biology and disease. Nature. 2009;461:1071–8.
19. Paull TT. Mechanisms of ATM activation. Annu Rev Biochem. 2015;84:711–38.
20. Polo SE, Jackson SP. Dynamics of DNA damage response proteins at DNA breaks: a focus on protein modifications. Genes Dev. 2011;25:409–33.
21. Blackford AN, Jackson SP. ATM, ATR, and DNA-PK: the trinity at the heart of the DNA damage response. Mol Cell. 2017;66:801–17.
22. Zimmermann M, De Lange T. 53BP1: Pro choice in DNA repair. Trends Cell Biol. 2014;24:108–17.
23. Kulkarni A, Wilson DM. The involvement of DNA-damage and -repair defects in neurological dysfunction. Am J Hum Genet. 2008;82:539–66.
24. Coppedè F. An overview of DNA repair in amyotrophic lateral sclerosis. ScientificWorldJournal. 2011;11:1679–91.
25. Konopka A, Atkin JD DNA Damage, Defective DNA repair, and neurodegeneration in amyotrophic lateral sclerosis. front aging neurosci. 2022; 14. https://doi.org/10.3389/fnagi.2022.786420.
26. Wang H, Kodavati M, Britz GW, Hegde ML DNA damage and repair deficiency in ALS/FTD-associated neurodegeneration: from molecular mechanisms to therapeutic implication. Front Mol Neurosci. 2021; 14. https://doi.org/10.3389/fnmol.2021.784361.
27. Gianini M, Bayona-Feliu A, Sproviero D, Barroso SI, Cereda C, Aguilera A. TDP-43 mutations link amyotrophic lateral sclerosis with R-loop homeostasis and R loopmediated DNA damage. PLoS Genet. 2020;16:1–23.
28. Hill SJ, Mordes DA, Cameron LA, Neuberg DS, Landini S, Eggan K, et al. Two familial ALS proteins function in prevention/repair of transcription-associated DNA damage. Proc Natl Acad Sci USA. 2016;113:E7701–9.
29. Wolozin B, Ivanov P. Stress granules and neurodegeneration. Nat Rev Neurosci. 2019;20:649–66.
30. Kuo WL, Meyn RE, Haidle CW. Neocarzinostatin-mediated DNA damage and repair in wild-type and repair-deficient Chinese hamster ovary cells. Cancer Res. 1984;44:1748–51.
31. Bañuelos A, Reyes E, Ocadiz R, Alvarez E, Moreno M, Monroy A, et al. Neocarzinostatin induces an effective p53-dependent response in human papillomavirus-positive cervical cancer cells. J Pharm Exp Ther. 2003;306:671–80.
32. Meyer B, Voss K-O, Tobias F, Jakob B, Durante M, Taucher-Scholz G. Clustered DNA damage induces pan-nuclear H2AX phosphorylation mediated by ATM and DNA–PK. Nucleic Acids Res. 2013;41:6109–18.
33. Ruiz S, Lopez-Contreras AJ, Gabut M, Marion RM, Gutierrez-Martinez P, Bua S, et al. Limiting replication stress during somatic cell reprogramming reduces genomic instability in induced pluripotent stem cells. Nat Commun. 2015;6:8036.
34. Moeglin E, Desplancq D, Conic S, Oulad-Abdelghani M, Stoessel A, Chiper M, et al. Uniform widespread nuclear phosphorylation of histone H2AX is an indicator of lethal DNA replication stress. Cancers (Basel). 2019;11:355.
35. Michelini F, Pitchiaya S, Vitelli V, Sharma S, Gioia U, Pessina F, et al. Damage-induced lncRNAs control the DNA damage response through interaction with DDRNAs at individual double-strand breaks. Nat Cell Biol. 2017;19:1400–11.
36. Zannini L, Delia D, Buscemi G. CHK2 kinase in the DNA damage response and beyond. J Mol Cell Biol. 2014;6:442–57.
37. de Feraudy S, Revet I, Bezrookove V, Feeney L, Cleaver JE. A minority of foci or pan-nuclear apoptotic staining of γH2AX in the S phase after UV damage contain DNA double-strand breaks. Proc Natl Acad Sci. 2010;107:6870–5.
38. Wood M, Quinet A, Lin YL, Davis AA, Pasero P, Ayala YM et al. TDP-43 dysfunction results in R-loop accumulation and DNA replication defects. J Cell Sci. 2020; 133. https://doi.org/10.1242/jcs.244129.
39. Pagano M, Pepperkok R, Verde F, Ansorge W, Draetta G. Cyclin A is required at two points in the human cell cycle. EMBO J. 1992;11:961–71.

40. Henglein B, Chenivesse X, Wang J, Eick D, Bréchot C. Structure and cell cycle-regulated transcription of the human cyclin A gene. Proc Natl Acad Sci. 1994;91:5490–4.
41. Sakaue-Sawano A, Kurokawa H, Morimura T, Hanyu A, Hama H, Osawa H, et al. Visualizing spatiotemporal dynamics of multicellular cell-cycle progression. Cell. 2008;132:487–98.
42. Mao Z, Bozzella M, Seluanov A, Gorbunova V. DNA repair by nonhomologous end joining and homologous recombination during cell cycle in human cells. Cell Cycle. 2008;7:2902–6.
43. Lee J-H, Cheong H-M, Kang M-Y, Kim S-Y, Kang Y. Ser1778 of 53BP1 plays a role in DNA double-strand break repairs. Korean J Physiol Pharm. 2009;13:343.
44. Jowsey P, Morrice NA, Hastie CJ, McLauchlan H, Toth R, Rouse J. Characterisation of the sites of DNA damage-induced 53BP1 phosphorylation catalysed by ATM and ATR. DNA Repair (Amst). 2007;6:1536–44.
45. Stucki M, Clapperton JA, Mohammad D, Yaffe MB, Smerdon SJ, Jackson SP. MDC1 directly binds phosphorylated histone H2AX to regulate cellular responses to DNA double-strand breaks. Cell. 2005;123:1213–26.
46. Lou Z, Minter-Dykhouse K, Franco S, Gostissa M, Rivera MA, Celeste A, et al. MDC1 maintains genomic stability by participating in the amplification of ATM-dependent DNA damage signals. Mol Cell. 2006;21:187–200.
47. Xie A, Hartlerode A, Stucki M, Odate S, Puget N, Kwok A, et al. Distinct roles of chromatin-associated proteins MDC1 and 53BP1 in mammalian double-strand break repair. Mol Cell. 2007;28:1045–57.
48. Ma Y, Farny NG. Connecting the dots: Neuronal senescence, stress granules, and neurodegeneration. Gene. 2023; 871. https://doi.org/10.1016/j.gene.2023.147437.
49. Shanbhag NM, Rafalska-Metcalf IU, Balane-Bolivar C, Janicki SM, Greenberg RA. An ATM-dependent transcriptional silencing program is transmitted through chromatin in Cis to DNA double strand breaks. Cell. 2010;141:970.
50. Iannelli F, Galbiati A, Capozzo I, Nguyen Q, Magnuson B, Michelini F, et al. A damaged genome's transcriptional landscape through multilayered expression profiling around in situ-mapped DNA double-strand breaks. Nat Commun. 2017;8:1–12.
51. Ji JH, Min S, Chae S, Ha GH, Kim Y, Park YJ, et al. De novo phosphorylation of H2AX by WSTF regulates transcription-coupled homologous recombination repair. Nucleic Acids Res. 2019;47:6299–314.
52. Ui A, Nagaura Y, Yasui A. Transcriptional elongation factor ENL phosphorylated by ATM recruits polycomb and switches off transcription for DSB repair. Mol Cell. 2015;58:468–82.
53. Pessina F, Giavazzi F, Yin Y, Gioia U, Vitelli V, Galbiati A, et al. Functional transcription promoters at DNA double-strand breaks mediate RNA-driven phase separation of damage-response factors. Nat Cell Biol. 2019;21:1286–99.
54. Francia S, Michelini F, Saxena A, Tang D, de Hoon M, Anelli V, et al. Site-specific DICER and DROSHA RNA products control the DNA-damage response. Nature. 2012;488:231–5.
55. Gioia U, Francia S, Cabrini M, Brambillasca S, Michelini F, Jones-Weinert CW, et al. Pharmacological boost of DNA damage response and repair by enhanced biogenesis of DNA damage response RNAs. Sci Rep. 2019;9:6460.
56. Lemaître C, Grabarz A, Tsouroula K, Andronov L, Furst A, Pankotai T, et al. Nuclear position dictates DNA repair pathway choice. Genes Dev. 2014;28:2450–63.
57. Don EK, Maschirow A, Radford RAW, Scherer NM, Vidal-Itriago A, Hogan A, et al. In vivo validation of bimolecular fluorescence complementation (BiFC) to investigate aggregate formation in amyotrophic lateral sclerosis (ALS). Mol Neurobiol. 2021;58:2061–74.
58. Francia S, Cabrini M, Matti V, Oldani A, d'Adda di Fagagna F. DICER, DROSHA and DNA damage response RNAs are necessary for the secondary recruitment of DNA damage response factors. J Cell Sci. 2016;129:1468–76.
59. Lu WT, Hawley BR, Skalka GL, Baldock RA, Smith EM, Bader AS et al. Drosha drives the formation of DNA:RNA hybrids around DNA break sites to facilitate DNA repair. Nat Commun. 2018; 9. https://doi.org/10.1038/s41467-018-02893-x.
60. Cabrini M, Roncador M, Galbiati A, Cipolla L, Maffia A, Iannelli F et al. DROSHA is recruited to DNA damage sites by the MRN complex to promote non-homologous end joining. J Cell Sci. 2021; 134. https://doi.org/10.1242/jcs.249706.
61. Paudel B, Jeong S-Y, Martinez CP, Rickman A, Haluck-Kangas A, Bartom ET, et al. Death Induced by Survival gene Elimination (DISE) correlates with neurotoxicity in Alzheimer's disease and aging. Nat Commun. 2024;15:264.
62. Mitra J, Guerrero EN, Hegde PM, Liachko NF, Wang H, Vasquez V, et al. Motor neuron disease-associated loss of nuclear TDP-43 is linked to DNA double-strand break repair defects. Proc Natl Acad Sci USA. 2019;116:4696–705.
63. Scarian E, Bordoni M, Fantini V, Jacchetti E, Raimondi MT, Diamanti L et al. Patients' stem cells differentiation in a 3D environment as a promising experimental tool for the study of amyotrophic lateral sclerosis. Int J Mol Sci. 2022; 23. https://doi.org/10.3390/ijms23105344.
64. Capauto D, Colantoni A, Lu L, Santini T, Peruzzi G, Biscarini S, et al. A regulatory circuitry between Gria2, miR-409, and miR-495 is affected by ALS FUS mutation in ESC-derived motor neurons. Mol Neurobiol. 2018;55:7635–51.
65. Shan G, Li Y, Zhang J, Li W, Szulwach KE, Duan R, et al. A small molecule enhances RNA interference and promotes microRNA processing. Nat Biotechnol. 2008;26:933–40.
66. Zhang Q, Zhang C, Xi Z. Enhancement of RNAi by a small molecule antibiotic enoxacin. Cell Res. 2008;18:1077–9.
67. Juan LS, Freije A, Sanz-Gómez N, Jiménez-Matías B, Pleguezuelos-Manzano C, Sanz JR, et al. DNA damage triggers squamous metaplasia in human lung and mammary cells via mitotic checkpoints. Cell Death Discov. 2023;9:21.
68. Krivega M, Zimmer J, Slezko A, Frank-Herrmann P, Rehnitz J, Hohenfellner M, et al. Genomic instability in individuals with sex determination defects and germ cell cancer. Cell Death Discov. 2023;9:1–14.
69. Milani M, Della Valle I, Rossi S, Fabbrizio P, Margotta C, Nardo G, et al. Neuroprotective effects of niclosamide on disease progression via inflammatory pathways modulation in SOD1-G93A and FUS-associated amyotrophic lateral sclerosis models. Neurotherapeutics. 2024;21:e00346.
70. Mitchell JC, McGoldrick P, Vance C, Hortobagyi T, Sreedharan J, Rogelj B, et al. Overexpression of human wild-type FUS causes progressive motor neuron degeneration in an age- and dose-dependent fashion. Acta Neuropathol. 2013;125:273–88.
71. Li Y, Ray P, Rao EJ, Shi C, Guo W, Chen X, et al. A Drosophila model for TDP-43 proteinopathy. Proc Natl Acad Sci USA. 2010;107:3169–74.
72. Lee YS, Nakahara K, Pham JW, Kim K, He Z, Sontheimer EJ, et al. Distinct roles for Drosophila Dicer-1 and Dicer-2 in the siRNA/miRNA silencing pathways. Cell. 2004;117:69–81.
73. Hou Y, Dan X, Babbar M, Wei Y, Hasselbalch SG, Croteau DL, et al. Ageing as a risk factor for neurodegenerative disease. Nat Rev Neurol. 2019;15:565–81.
74. He D, Xu Y, Liu M, Cui L. The inflammatory puzzle: piecing together the links between neuroinflammation and amyotrophic lateral sclerosis. Aging Dis. 2023;15:96–114.
75. Pessina F, Gioia U, Brandi O, Farina S, Ceccon M, Francia S, et al. DNA damage triggers a new phase in neurodegeneration. Trends Genet. 2021;37:337–54.
76. Mastrocola AS, Kim SH, Trinh AT, Rodenkirch LA, Tibbetts RS. The RNA-binding protein fused in sarcoma (FUS) functions downstream of poly(ADP-ribose) polymerase (PARP) in response to DNA damage. J Biol Chem. 2013;288:24731–41.
77. Wang H, Guo W, Mitra J, Hegde PM, Vandoorne T, Eckelmann BJ, et al. Mutant FUS causes DNA ligation defects to inhibit oxidative damage repair in Amyotrophic Lateral Sclerosis. Nat Commun. 2018;9:3683.
78. Ratti A, Gumina V, Lenzi P, Bossolasco P, Fulceri F, Volpe C, et al. Chronic stress induces formation of stress granules and pathological TDP-43 aggregates in human ALS fibroblasts and iPSC-motoneurons. Neurobiol Dis. 2020;145:105051.
79. D'Alessandro G, d'Adda di Fagagna F. Transcription and DNA damage: holding hands or crossing swords?. J Mol Biol. 2017;429:3215–29.
80. Hoppe-Seyler F, Butz K. Repression of endogenous p53 transactivation function in HeLa cervical carcinoma cells by human papillomavirus type 16 E6, human mdm-2, and mutant p53. J Virol. 1993;67:3111–7.
81. Lopes I, Altab G, Raina P, de Magalhães JP. Gene size matters: an analysis of gene length in the human genome. Front Genet 2021; 12. https://doi.org/10.3389/fgene.2021.559998.
82. Zylka MJ, Simon JM, Philpot BD. Gene length matters in neurons. Neuron. 2015;86:353.
83. Hatchi E, Goehring L, Landini S, Skourti-Stathaki K, DeConti DK, Abderazzaq FO, et al. BRCA1 and RNAi factors promote repair mediated by small RNAs and PALB2–RAD52. Nature. 2021;591:665–70.
84. Carpenter AE, Jones TR, Lamprecht MR, Clarke C, Kang IH, Friman O, et al. CellProfiler: image analysis software for identifying and quantifying cell phenotypes. Genome Biol. 2006;7:R100.
85. Bolte S, Cordelières FP. A guided tour into subcellular colocalization analysis in light microscopy. J Microsc. 2006;224:213–32.
86. Esposito F, Capozzo I, Modafferi S, Gioia U, Manfredi L, Iannelli F et al. DROSHA, DICER and Damage-Induced long ncRNA control BMI1-dependent transcriptional repression at DNA double-strand break. bioRxiv 2024; 2024.08.07.606960 https://doi.org/10.1101/2024.08.07.606960.
87. Morello G, Cancila V, La Rosa M, Germano G, Lecis D, Amodio V, et al. T cells expressing receptor recombination/revision machinery are detected in the tumor microenvironment and expanded in genomically over-unstable models. Cancer Immunol Res. 2021;9:825–37.
88. Potter CJ, Huang H, Xu T. Drosophila Tsc1 functions with Tsc2 to antagonize insulin signaling in regulating cell growth, cell proliferation, and organ size. Cell. 2001;105:357–68.

ACKNOWLEDGEMENTS

We would like to thank Dr Simone Sabbioneda (IGM-CNR, Pavia) for support with the fluorescence-activated cell sorting; Dr Sara Tavella (IGM-CNR, Pavia) and Dr Sara Sepe (IFOM, Milan) for their helpful advice; Giulia Vitali and Martina Battistoni (IGM-CNR,

Pavia) for technical support; the Imaging Facility at the Center for Life Nano & NeuroScience, Istituto Italiano di Tecnologia. SM is supported by Istituto Universitario di Studi Superiori (IUSS, Pavia, Itay). SFa is supported by Fondazione Umberto Veronesi. FE is supported by the AIRC fellowship "Guglielmina Lucatello e Gino Mazzega" 2021 (Ref. 26700). SD'U is supported by ERC-2019-SyG 855923-ASTRA. ES and OP are supported by Italian Ministry of Health (Ricerca Corrente 2022–2024). ND'A is supported by: Fondazione AriSLA ETS (Fondazione di Ricerca per la SLA ETS), SwitchALS project; #NEXTGENERATIONEU (NGEU) and founded by the Ministry of University and Research (MUR), National Recovery and Resilience Plan (NRRP), project MNESYS (PE0000006) – A Multiscale Integrated Approach to the Study of the Nervous System in Health and Disease (DN. 1553 11.10.2022). MC is supported by: Fondazione AriSLA ETS (Fondazione di ricerca per la SLA ETS), SwitchALS project; CNR (DBA.AD005.225-NUTRAGE-FOE2021). GCe is supported by: CNR (DBA.AD005.225-NUTRAGE-FOE2021); CNR (Flagship Project Interomics); EU funding within the MUR PNRR "National Center for Gene Therapy and Drugs based on RNA Technology" (# CN00000041 CN3 RNA). Fd'AdF is supported by: ERC advanced grant (TELORNAGING —835103); AIRC-IG(21762); Telethon (GGP17111); AIRC 5 × 1000 (21091); Progetti di Ricerca di Interesse Nazionale (PRIN) 2017 (2017NWEXEP); PRIN 2020 (2020CXFL4T); PRIN 2022 (2022R7LH5T); Progetto AriSLA 2016 "DDRNA&ALS and 2021 "DDR&ALS" (FG_24/2020); POR FESR 2014-2020 Regione Lombardia (InterSLA project) (DSB.AD004.294); FRRB—Fondazione Regionale per la Ricerca Biomedica—under the frame of EJP RD, the European Joint Program on Rare Diseases with funding from the European Union's Horizon 2020 research and innovation program under the EJP RD COFUND-EJP NO 825575 (EJPRD19-206); co-funding European Union – Next Generation EU, in the context of The National Recovery and Resilience Plan, Investment Partenariato Esteso PE8 "Conseguenze e sfide dell'invecchiamento", Project Age-It (Aging Well in an Aging Society) GAE 492 PNRR PE_8 SPOKE 2; PNRR-CN3 "National Center for Gene Therapy and Drugs based on RNA Technology"; ERC POC TELOVACCINE—101113229; Telethon GMR23T2007. UG is supported by: Progetto AriSLA 2016 "DDRNA&ALS and 2021 "DDR & ALS"; PRIN 2020 CXFL4T; Istituto Superiore di Sanità RIPREI2023_7c8ae10d783c. SFr is supported by: Progetto AriSLA 2016 "DDRNA&ALS" and 2021 "DDR&ALS"; PNRR-CN3 "National Center for Gene Therapy and Drugs based on RNA Technology"; POR FESR 2014-2020 Regione Lombardia (InterSLA project).

AUTHOR CONTRIBUTIONS

SM performed the immunoblot analyses of TDP-43 and FUS protein levels; carried out quantitative immunofluorescence (IF) studies for pATM, pCHK2, 53BP1, p53BP1, MDC1, DROSHA and DICER in HeLa cells; analyzed dilncRNA expression; performed the experiments in FUCCI HeLa and in HT-22 cells; conducted the IF analyses in hMNPs and mMNs and edited the manuscript. SFa carried out IF analysis for quantification of WT and mutant FUS CIs; experiments of colocalization between FUS and stress granules; IF analysis of γH2AX signals with and without ATM and ATR inhibitors, analysis of pATM, 53BP1 and p53BP1 signals in cells expressing WT and mutant FUS and immunoblot experiments for FUS expression upon transfection in HeLa cells. FE performed ATM and ATR inhibition experiments; BrdU and CycA staining; EU incorporation assays; IF and RT-qPCR analysis for DROSHA expression; enoxacin treatment experiments and generated the constructs for the BiFC assays. OB carried out the experiments concerning the impact of mutant TDP-43 isoforms on cytoplasmic inclusion and stress granule formation, conducted the experiments in SH-SY5Y cells and studied DDR activation following $NaAsO_2$ administration. MDS carried out the experiments involving *Drosophila melanogaster* strains. IDV conducted the experiments in mice and generated the spinal cord tissues from such animals. SD'U generated mMNs, performed IF analyses on such samples and edited the manuscript. ES generated hMNPs and edited the manuscript. GCi performed IHC analyses on murine specimens. AR carried out the EU incorporation assays with ATM inhibitors. FP conducted the IHC staining in murine samples. AG contributed to confocal microscopy studies, carried out the co-localization analyses, assisted SM with the fluorescence-activated cell sorting and edited the manuscript. TS performed confocal microscopy analyses on mMNs. OP coordinated the experiments in hMNPs, supervised ES and edited the manuscript. MM coordinated the experiments in mMNs, supervised S.D'U and edited the manuscript. ND'A and MC coordinated the experiments in hFUS mice, supervised IDV and edited the manuscript. GCe coordinated the analyses in *Drosophila melanogaster* strains, supervised MDS and edited the manuscript. Fd'AdF participated in designing the study and edited the manuscript. UG conceived, conducted and analyzed the comet assays; contributed to the study design, assembled and revised the manuscript. SFr conceived the study, coordinated experimental activities, wrote and edited the manuscript.

COMPETING INTERESTS

The authors declare no competing interests.

ETHICAL APPROVAL

Mice used in this study were housed at the Tor Vergata University Animal Facility (CIMETA) in accordance with the FELASA Recommendations, European Guidelines for the use of animals in research (2010/63/EU), and Italian Laws (D.L. 26/2014). All experiments were conducted in compliance with the ARRIVE guidelines, with the approval by the local ethics committee and the Italian Ministry of Health.

ADDITIONAL INFORMATION

Supplementary information The online version contains supplementary material available at https://doi.org/10.1038/s41418-025-01530-7.

Correspondence and requests for materials should be addressed to Ubaldo Gioia or Sofia Francia.

Reprints and permission information is available at http://www.nature.com/reprints

Publisher's note Springer Nature remains neutral with regard to jurisdictional claims in published maps and institutional affiliations.